CAMK1D triggers immune resistance of human tumor cells refractory to anti-PD-L1 treatment

Valentina Volpin,[1,2] Tillmann Michels,[1,2,3] Antonio Sorrentino[1,2], Ayse N. Menevse[1], Gertrud Knoll[4], Madlen Ditz[1], Vladimir M. Milenkovic[5], Chih-Yeh Chen[1], Anchana Rathinasamy[1], Klaus Griewank[6], Michael Boutros[7], Sebastian Haferkamp[8], Mark Berneburg[8], Christian H. Wetzel[5], Anja Seckinger[9], Dirk Hose[10], Hartmut Goldschmidt[11], Martin Ehrenschwender[4], Mathias Witzens-Harig[12], Arpad Szoor[13], Gyorgy Vereb[13], Nisit Khandelwal[3] and Philipp Beckhove[1,2,14]

Affiliations

[1]Regensburg Center for Interventional Immunology (RCI), University Regensburg, Regensburg, 93053, Germany
[2]German Cancer Research Center (DKFZ), Translational Immunology, Heidelberg, 69120, Germany
[3] iOmx Therapeutics AG, 82152 Martinsried/Munich, Germany
[4]Institute of Clinical Microbiology and Hygiene, University Hospital Regensburg, 93053, Germany
[5]Department of Psychiatry and Psychotherapy, Molecular Neurosciences, University of Regensburg, 93053 Regensburg, Germany
[6]Department of Dermatology, University Hospital Essen, West German Cancer Center, University Duisburg-Essen and the German Cancer Consortium, Essen, Germany
[7]German Cancer Research Center (DKFZ), Division Signalling and Functional Genomics, Heidelberg, 69120, Germany
[8]Department of Dermatology, University Hospital Regensburg, Regensburg, 93053, Germany
[9]Labor für Myelomforschung, Medizinische Klinik V, Universitätsklinikum Heidelberg, 69120 Heidelberg, Germany
[10]Department of Hematology and Immunology, Myeloma Center Brussels, Laarbeeklaan 103, 1090 Jette, Belgium[11]Department of Internal Medicine V and National Center of Tumor Diseases (NCT), University Hospital Heidelberg, 69120 Heidelberg, Germany
[12]Department of Hematology, Oncology and Rheumatology, University Hospital Heidelberg, 69120 Heidelberg, Germany
[13]Department of Biophysics and Cell Biology, Faculty of Medicine, University of Debrecen, 4032 Debrecen Hungary

[14]Department of Hematology, Oncology, Internal Medicine 3. University Hospital Regensburg, Regensburg, 93053, Germany

Running title

CAMK1D triggers immune resistance by caspase inhibition

Funding

This project was funded by the Deutsche Forschungsgemeinschaft (DFG, German Research Foundation) - Projektnummer 324392634 - TRR 221 and the National Research, Development and Innovation Office, Hungary - OTKA K119690.

Correspondence to: Philipp Beckhove, Regensburg Center for Interventional Immunology University Regensburg, Franz-Josef-Strauss-Allee 11, D-93053 Regensburg, Phone: +49-941- 944 38101, Email: beckhove@rcii.de

Abstract

The success of cancer immunotherapy is limited by resistance to immune-checkpoint blockade. We therefore conducted a genetic screen to identify genes that mediated resistance against cytotoxic T lymphocytes (CTL) in anti-PD-L1 treatment refractory human tumors. Using PD-L1 positive multiple myeloma cells co-cultured with tumor-reactive bone marrow-infiltrating CTL as a model, we identified calcium/calmodulin-dependent protein kinase 1D (CAMK1D) as a key modulator of tumor intrinsic immune resistance. CAMK1D was co-expressed with PD-L1 in anti-PD-L1/PD-1 treatment refractory cancer types and correlated with poor prognosis in these tumors. CAMK1D was activated by CTL through Fas-receptor stimulation, which led to CAMK1D binding to and phosphorylating caspase -3, -6 and -7, inhibiting their activation and function. Consistently, CAMK1D mediated immune resistance of murine colorectal cancer cells *in vivo*. The pharmacological inhibition of CAMK1D on the other hand, restored the sensitivity towards Fas-ligand treatment in multiple myeloma and uveal melanoma cells *in vitro*. Thus, rapid inhibition of the terminal apoptotic cascade by CAMK1D expressed in anti-PD-L1 refractory tumors via T cell recognition may have contributed to tumor immune resistance.

Introduction

Endogenous T cell responses against tumor antigens occur frequently in a broad variety of cancer types (1-3). Although these T cell responses correlate to improved patient prognoses (2, 4, 5), they often do not rescue patients from tumor progression. A major reason, lies in the capacity of tumor cells to regulate T cell activity through expression of the immune-inhibitory ligand PD-L1. The latter stimulates the inhibitory receptor PD-1 expressed on effector T cells and reduces T cell receptor signaling (6). PD-L1 expression in healthy and tumor tissues can be induced by inflammatory cytokines such as IFN-gamma by effector T cells (7-9) and serves as a mechanism to prevent autoimmune diseases (10). Consequently, blockade of PD-L1/PD-1 interactions by therapeutic antibodies has resulted in stunning immune rejection of tumors in many patients (11-14). Still, a significant proportion of cancer patients lack responses to anti-PD-L1/PD-1 therapies (15-17) possibly due to impaired IFN-gamma responsiveness resulting in reduced PD-L1 expression, severe and irreversible T cell exhaustion, or PD-1-induced blockade of T cell differentiation (18). However, since functional tumor reactive T cells are found in many patients refractory to anti-PD-L1/PD-1 treatment (3, 5), these mechanisms may only explain immune response resistance in a minor fraction of cases. Additional immune regulatory interactions may impose protection against immune destruction. Several immune inhibitory receptors such as TIM3 or VISTA, triggered by ligands expressed in tumors, are characterized (19, 20), but immune resistance is likely caused by more than immune regulatory ligands controlling T cell activity such as tumor cell intrinsic resistance mechanisms.

Multiple myeloma (MM) is a rarely curable B-cell malignancy characterized by the accumulation of malignant plasma cell clones in the bone marrow (21). In MM, spontaneous cytotoxic T cell responses against myeloma-associated antigens occur (1). Immune-checkpoint molecules are

expressed by myeloma cells and induce tumor-related immune suppression (22-24). PD-L1 is commonly expressed on malignant plasma cells (9) and high expression of PD-L1 associates with disease progression and is upregulated at relapse or in the refractory stage (25). Nevertheless, results of a phase I trial with PD-1 blocking antibodies reported no objective responses amongst the 27 treated MM patients (26). There is thus rationale to assume that other immune-checkpoint molecules may play a role in tumor escape mechanisms. Various immunotherapeutic treatments are being tested in MM, including antibodies against CD38 (e.g. daratumumab, isatuximab), SLAMF7 (elotuzumab), BCMA-CAR-T-based treatments or BCMA-T-cell bispecific antibodies (27-31).

Here, we performed a systematic search for genes that regulated immune responsiveness in tumor cells, using MM as anti-PD-L1/PD-1 treatment unresponsive tumor model (26).

In order to identify genes that inhibit tumor immune destruction by CTL, we applied a high-throughput (HTP) genetic screen allowing the silencing of a multitude of genes and subsequently assessed tumor lysis by patient-derived marrow-infiltrating lymphocytes (MILs). We identified 90 genes that regulated immune responsiveness after cytotoxic T cell attack. Among them, Calcium/Calmodulin Dependent Protein Kinase 1D (CAMK1D) was co-expressed with PD-L1 and protected against T cell-induced tumor cell killing in MM and other PD-L1 refractory human cancers.

Materials and Methods

Experimental model and subject details: Patients, healthy donors, and samples

Patients with previously untreated multiple myeloma (n=332) or monoclonal gammopathy of unknown significance (MGUS; n=22) at the University Hospitals of Heidelberg and Montpellier

as well as 10 healthy normal donors were included in this study, which was approved by the ethics committee (#229/2003 and S-152/2010) after written informed consent. Patients were diagnosed, staged and response to treatment assessed according to standard criteria (32-34).

Samples: Normal bone marrow plasma cells and myeloma cells from the aforementioned patients were purified using anti-CD138 microbeads (Miltenyi Biotec, Bergisch Gladbach, Germany #130-051-301) from bone marrow aspirates previously published (35, 36). Peripheral $CD27^+$ memory B-cells (n=11) were FACS-sorted as described (37). The human myeloma cell lines U266, RPMI-8226, LP-1, OPM-2, SK-MM-2, AMO-1, JJN-3, NCI-H929, KMS-12-BM, KMS-11, KMS-12-PE, KMS-18, MM1.S, JIM3, KARPAS-620, L363 and ANBL6 were purchased from the German Collection of Microorganisms and Cell Cultures (Braunschweig, Germany) and the American Type Cell Culture (Wesel, Germany), the XG-lines were generated at INSERM U1040 (Montpellier, France) (38). KMM-1 cells were obtained from the National Institutes of Biomedical Innovation, Health and Nutrition (Osaka, Japan). Cell line identity was regularly assessed by DNA-fingerprinting and compared to the initial sample. Cell lines were grown from initial of first passage aliquots on a regular basis. Mycoplasma-contamination excluded by PCR-based assays, and EBV-infection status by clinical routine PCR-based diagnostics. If not otherwise stated, cell lines used for expression profiling were assessed from initial or early passage aliquots. Polyclonal plasmablastic cells (n=10) were generated as published (36, 39, 40). The human uveal melanoma cell line Mel270 was established, characterized and provided by Prof. Griewank (University Hospital Essen) (41). KMM-1-luc cells were generated after transfection with a pEGFP-luc plasmid (provided by Dr. Rudolf Haase, LMU Munich, Germany) and selected for the G418-resistance gene. Lipofectamine LTX with Plus reagent (Thermo Scientific #15338100) were used as transfection reagents according to the manufacturer´s instructions. Transfected cells were

selected for 14 days with G418-containing medium (0.6 mg/mL). KMM-1-luc cells were sorted twice for the expression of GFP by flow cytometry (with 87% and 100% purity, respectively) and cultured in the presence of 0.6 mg/mL G418. Cell sorting was conducted in collaboration with the DKFZ sorting core facility, using the FACSARIA II cell sorter (BD) and data were analyzed using FlowJo (Tree Star). KMM-1, U266 and Mel270 were cultured under standard conditions in RPMI media supplemented with 10% fetal calf serum, 100 U/ml penicillin G and 100 µg/ml streptomycin at 37 °C in a humidified atmosphere under 5% CO_2.

Isolation of peripheral blood mononuclear cells (PBMCs)

PBMCs were isolated from buffy coats of healthy donors via biocoll density gradient centrifugation (Biochrome). Briefly, buffy coats were diluted 1:10 in RPMI and added to 50 mL conical centrifuge tubes, containing 15 mL of biocoll solution. Density gradient centrifugation was performed at 2000 rpm for 20 min at room temperature using low brake. Afterwards, PBMCs were collected, washed twice with RPMI and frozen in aliquots of 5 x 10^7 cells per vial using freezing media A-B (1:1) (Freezing medium A: 60% AB-serum + 40% RPMI; Freezing medium B: 80% AB-serum + 20% DMSO).

MILs isolation

Marrow-infiltrating lymphocytes were isolated from the bone marrow of a multiple myeloma patient. Briefly, T cells were isolated from the negative fraction of CD138-sorted bone marrow cells using Untouched Human T cells Dynabeads (Invitrogen #11344D) following manufacturer's instructions. Cells were stained for anti-CD3 (Pacific Blue™ anti-human CD3 (Clone OKT3), Biolegend), anti-CD4 (APC/Cy7 mouse anti-human CD4 (Clone RPA-T4), BD Biosciences) and

158 anti-CD8 (Pacific Blue™ mouse anti-human CD8 (Clone RPA-T8), BD Biosciences), tested for
159 HLA-A2 positivity (APC mouse anti-human HLA-A2 Clone BB7.2 (RUO), BD Biosciences) via
160 flow cytometry and subsequently expanded using the rapid expansion protocol as described below.
161
162 **MILs expansion**
163 MILs cultures were ex-vivo expanded using a modified version of the Rapid Expansion Protocol
164 (REP) (42, 43). $2x10^6$ of freshly isolated MILs were diluted to 6 $x10^5$ cell/mL in CLM
165 supplemented with 3000 U/mL rHuIL2 (Novartis Pharma). Cells were incubated in 25 cm^2 tissue
166 culture flask for 48h at 37°C and 5% CO_2. An excess of irradiated allogeneic PBMC from healthy
167 donors were added as "feeder cells" to support the activation and propagation of T cells early
168 during the REP (44). Thus, PBMCs from three different buffy coats (at a ratio of 1:1:1) were
169 irradiated with 60 Gy (Gammacell 1000) and used as feeder cells to support MILs expansion.
170 $2x10^6$ MILs were co-incubated with $2x10^8$ feeder cells (in a ratio 1:100) in 400 mL of MIL
171 expansion medium (CLM/AIM-V) with 30 ng/mL OKT3 antibody (Thermo Scientific) and 3000
172 IU/mL IL-2 for 5 days in a G-Rex 100 cell culture flask. Afterwards, 250 mL of supernatant was
173 replaced with 150 mL of fresh media and IL-2 was replenished to keep the concentration at 3000
174 IU/mL. On day 7, MILs were divided into three G-Rex 100 flasks in a final volume of 250 mL
175 medium each and media was again replenished on day 11. On day 14 of the expansion, MILs were
176 counted and frozen in aliquots of $40x10^6$ cells/mL in freezing media A (60% AB serum and 40%
177 RPMI1640) and B (80% AB serum and 20% DMSO).
178
179 **Generation of flu-antigen specific $CD8^+$ T cells**

For the generation of flu-specific $CD8^+$ T cells (flu TC), PBMCs from HLA-A2 healthy donors were isolated as described above. Total $CD8^+$ T cells were sorted from PBMCs by magnetic separation (Miltenyi #130-096-495) (day 0) according to the manufacturer's instructions and expanded in the presence of A2-matched flu peptide (GILGFVFTL) for 14 days.

The autologous and peptide-loaded CD8 negative fraction was irradiated with 60 Gray (IBL 437C Blood Irradiator) and used as feeder cells for 1 week. Afterwards, these cells were substituted with irradiated (60 Gray; IBL 437C Blood Irradiator) T2 cells and used as fresh feeder cells. On day 1 and day 8, 100 IU/mL IL2 (Novartis Pharma) and 5 ng/μL IL15 (R&D Systems) were added to the expansion. The percentage of flu-antigen specific T cells was determined by pentamer staining (GILGFVFTL-APC, ProImmune #P007-0A-E) on day 7 and 14 via flow cytometry analysis according to the manufacturer's instructions. After antigen-specific expansion, flu TC were sorted by FACS and expanded further for 14 days by using the rapid expansion protocol.

PCR and qPCR

Gene expression was measured using end-point Polymerase Chain Reaction (PCR). Briefly, total RNA was isolated from cell pellets using the RNeasy Mini kit (Qiagen #74106) according to the manufacturer's guidelines. RNA quality and concentration were analyzed using the Scan Drop (AnalytikJena). 1 μg of RNA was reverse transcribed to complementary DNA (cDNA) using the QuantiTect reverse transcription kit (Qiagen #205313) according to the manufacturer's protocol. Synthesized cDNA was amplified using conventional PCR. PCR samples were set up in a 25 μL volume using 2x MyTaq HS Red Mix (Bioline #BIO-25044), 500 nM of gene-specific primer mix (supplementary Table 2) and 100 ng of template cDNA. Water was added to the reaction mix instead of cDNA for contamination controls. The PCR program was set as the following: 95°C for

3 min, 35 cycles of 3 repetitive steps of denaturation (95°C for 30 s), annealing (60°C for 30 s) and extension (72°C for 30 s), and a final step at 72°C for 5 min. PCR products were run on a 2% agarose gel in Tris-acetate-EDTA (TAE) buffer (ThermoFisher Scientific #B49) using a gel electrophoresis system (Thermo Scientific) and DNA bands were visualized using UV light of myECL Imager (Thermo Scientific).

Knockdown efficiency of siRNA sequences was measured by quantitative PCR (qPCR). For qPCR, 10 ng of template cDNA, 2x QuantiFast SYBR Green PCR mix (Qiagen #204056) and 300 nM of gene-specific primer mix (supplementary Table 2) was used per 20 μL reaction and each sample was prepared in triplicates. Reactions were run using the QuantStudio 3 (Applied Biosystems). Gene expression was normalized to β-actin and results were shown as fold change. The analysis was performed using comparative Ct method.

Gene expression profiling

Gene expression profiling was performed using U133 2.0 plus arrays (Affymetrix, Santa Clara, CA, USA) as published (35, 45, 46). Expression data are deposited in ArrayExpress under accession numbers E-MTAB-317.

Survival and correlation analysis using The Cancer Genome Atlas (TCGA)

Transcriptomic gene expression (RNASeqV2, RSEM) and clinical data from all available tumor entities was downloaded from TCGA (using getTCGA function of TCGA2STAT (version 1.2) package for R (47). Log2-normalized expression values for uveal melanoma (TCGA-UVM, 80 patients), ovarian cancer (TCGA-OV, 303 patients), stomach adenocarcinoma (TCGA-STAD) and stomach and esophageal carcinoma (TCGA-STES, 599 patients) were correlated (Person's r) using

the ggpubr package for R. Survival curves were generated using survminer package for R. FAS expression was cut at the median to generate Fas high and low sets. Similarly, CAMK1D expression was cut at the median for the Kaplan-Meier survival curves. Significance was calculated using the log-rank test.

Reverse siRNA transfection

Gene knockdown in tumor cells was induced using reverse siRNA transfection with Lipofectamine RNAiMAX (Thermo Scientific #13778-150). Briefly, 200 µL of 250 nM siRNA solution (supplementary Table 2) was added to each well of a 6-well plate. 4 µl of RNAiMAX transfection reagent was diluted in 196 µL of RPMI (Sigma-Aldrich) and incubated for 10 min at room temperature (RT). 400 µL of additional RPMI was added and 600 µL of RNAiMAX mix was given to the siRNA coated wells and incubated for 30 min at RT. 3,5 x 10^5 KMM-1 (WT or luc) cells were resuspended in 1,2 mL of antibiotic-free RPMI culture medium supplemented with 10% FCS, seeded in the siRNA-RNAiMAX containing wells and incubated for 48 h at 37°C, 5% CO_2. Final siRNA concentration was 25 nM in all cases.

Phospho-Protein Isolation

To isolate phosphorylated proteins from cells, tumor cells were pelleted at 0.5 x g for 5 min and washed once with PBS at 4°C. The cell pellets were lysed with one pellet volume of Phosphoplex Lysis Buffer (Merck Millipore #43-040) containing protease inhibitor cocktail (Cabliochem #539134, 1:100) and phosphatase inhibitor cocktail (Sigma-Aldrich #P0044, 1:100) at 4 °C for 15 min on a rotator. Samples were centrifuged at 17000 g at 4°C for 15 min. Supernatants containing

the protein lysates were collected into fresh tubes and quantified using the Pierce BCA Protein Assay Kit (Thermo Scientific #23225) according to the manufacturer's protocol.

Briefly, supernatants were diluted 1:5 in water and pipetted together with BCA-standards into a 96-well plate. BCA solution A and B were mixed 50:1 and 200 µl of this mix was added to each well. After 30 min incubation at 37 °C, the absorbance at 562 nm was measured with the TECAN reader and the protein concentration of the samples was calculated using the standard curve. Proteins were stored at -20 °C.

SDS-PAGE

30 µg of protein lysates were denaturated in 4x NuPAGE LDS Sample Buffer (Thermo Scientific #NP0008) containing 10% ß-mercaptoethanol (Sigma-Aldrich #M6250-100ML) at 70 °C for 10 min. Samples were spun down and separated on NuPAGE 4-12% Bis-Tris Gels (Thermo Scientific NP0321BOX) along with PageRuler Prestained Protein Ladder (Thermo Scientific #26616) and run at 115-150 V for 90 min using 1X MES running buffer (Life Technologies #NP0002).

Semi-Dry Western Blot

Proteins were transferred from the gel to a PVDF membrane (Millipore #ISEQ00010) using a semi-dry western blot method. Briefly, the PVDF blotting membrane was activated in 100% methanol (Millipore) for 1 min and afterwards placed in Pierce 1-Step Transfer Buffer (Thermo Science #84731X5) until use. Blots were assembled from anode to cathode into the Pierce Power Blot cassette (Thermo Scientific) and run at 24 V for 10 min. Membranes were washed in 1x TBS and then placed in blocking solution (5% BSA / 0.05% TBST) for 2 h. Primary antibodies (anti-CAMK1D (Abcam #ab172618) 1:20000, anti-caspase-3 (Abcam #ab32351) 1:750, anti-caspase-

6 (Abcam #ab108335) 1:2000, anti-caspase-7 (Thermo Scientific MA5-15159) 1:1000, anti-caspase-3 (phospho S150) (Abcam #ab59425) 1:850, anti-caspase-6 (phospho S257) (Abcam #ab135543) 1:250 and sodium potassium ATPase (Abcam #ab76020) 1:20000) were diluted in 5% BSA / 0.05% TBST and kept on the membrane overnight at 4 °C on a rotator. Membranes were then washed three times for 10 min with 1 % BSA / 0.05% TBST. Afterwards, HRP-conjugated secondary antibodies (anti-rabbit 1:4000, Cell Signaling #7074 or anti-mouse 1:4000, Cell Signaling #7076) were added to 1% BSA/TBST and kept on the membrane at room temperature for 1h on a shaker. Thereafter, the membranes were washed for 10 min with 1% BSA/TBST, then TBST and lastly with TBS. The blots were incubated with the Amersham ECL Western Blotting Detection Reagent (Reagent A and Reagent B, 1:1, GE Healthcare # RPN2109) for 4 min and the chemiluminescence was detected with myECL Imager (Thermo Scientific). Images were analyzed using the ImageJ software (Wayane Rasband).

Co-immunoprecipitation assay

For detection of direct protein-protein interaction, co-immunoprecipitation was performed. Briefly, 10 M tumor cells were seeded in 10 cm^2 petri dishes. The next day, cells were stimulated for 4 h with 100 ng/ml rHuFasL (Biolegend #589404). Unstimulated cells were used as negative control. Afterwards, tumor cells were detached, resuspended in ice cold TBS and centrifuged at 400 g for 6 min at 4°C. Supernatant was discarded, cell pellet was resuspended in 1,5 mL TBS and centrifuged at 500 g for 8 min at 4°C. Cell pellet was lysed with 1,5 mL lysis buffer (50 mM Tris-HCl, 150 mM NaCl, 0,5% NP40 or Triton-X) containing protease inhibitor (Millipore #539134-1 ML) and kept on a rotator for 1 h at 4°C. Afterwards, cells were centrifuged for 20 min at 20000 g at 4°C. Supernatant was collected and centrifuged for further 5 min at 20000 g at 4°C. Protein-

G agarose (Sigma-Aldrich) was washed with 1 mL TBS and centrifuged for 1 min at 12000 g. 1 mL of cell supernatant containing cytoplasmatic proteins was added to 60 µL protein-G agarose (Sigma-Aldrich #11719416001), incubated with caspase-3 (1:50) (Cell Signaling #9662), caspase-6 (1:50) (Abcam #ab108335) or caspase-7 (1:100) (Cell Signaling #9491) antibodies and incubated overnight on a rotator at 4°C. 90 µL of cell lysates were frozen at -20°C. The next day, the immunoprecipitated samples were centrifuged at 12000 g at 4°C for 1 min. Supernatant was discarded and protein-G agarose was washed three times with lyses buffer and centrifuged at 12000 g at 4°C for 1 min. 2x LDS containing 10% β-mercaptoethanol was added to the immunoprecipitated samples, while 4x LDS containing 10% β-mercaptoethanol was added to the lysates. Samples were denaturated for 10 min at 95°C on a thermocycler. Samples were spun down and separated on NuPAGE 4-12% Bis- Tris Gels (Thermo Scientific #NP0335BOX) along with PageRuler Prestained Protein Ladder (Thermo Scientific #26616) and run at 115-150 V for 90 min. After electrophoresis, proteins were transferred on a PVDF membrane (Millipore). CAMK1D antibody (1:10000) was diluted in 5% BSA / 0.05% TBST and kept on the membrane overnight at 4°C on a rotator. Membranes were then washed three times for 10 min with 1% BSA / 0.05% TBST. Afterwards, HRP-conjugated secondary antibodies (anti-rabbit 1:3000) was added to 1% BSA / TBST and kept on the membrane at room temperature for 1 h on a shaker. The membrane was washed. The blot was incubated with the ECL Detection Reagent (Reagent A and Reagent B, 1:1, GE Healthcare) for 4 min and the chemiluminescence was detected with myECL Imager (Thermo Scientific). Images were analyzed using the ImageJ software (Wayane Rasband).

Plasmid transfection

316 To generate KMM-1-luc cells, 3,5 x 10^5 KMM-1 WT cells were seeded in a 6 well plate and
317 incubated at 37°C overnight. 15 µL Lipofectamine LTX reagent were diluted in 150 µL Opti-MEM
318 medium (Gibco). Simultaneously, 3.5 µg of pEGFP-Luc plasmid was diluted in 175 µL Opti-MEM
319 medium and 3.5 µL of Plus Reagent was added. 150 µL of diluted DNA was added to 150 µL
320 diluted Lipofectamine LTX (Life Technologies) reagent and incubated for 5 min at RT. DNA-lipid
321 complex was then added to the growth medium of the myeloma cells. Cells were incubated at 37°C
322 for 48 h before investigation of transfection efficacy by flow cytometry.
323
324 **Luciferase-based cytotoxicity assay**
325 KMM-1-luc cells were reverse transfected with the desired siRNA sequences (supplementary
326 Table 2) in white 96-well-plate (Perkin Elmer) and incubated for 48 h at 37°C, 5% CO_2. On the
327 same day of transfection, MILs were thawed and treated with benzonase (100 IU/mL) (Merck).
328 Cell density was adjusted to 0.6 x 10^6 cells/mL in CLM supplemented with 3000 IU/mL rhuIL-2
329 (Novartis) for 48 h. IL-2 was depleted 24 h before the co-culture. Briefly, cells were collected,
330 centrifuged at 1400 rpm for 10min, and resuspended in CLM at a concentration of 0.6 x 10^6
331 cells/mL. Flu TC were thawed 6 h before co-culture. For the cytotoxicity assays, MILs, flu TC,
332 the supernatant of activated MILs, or rHuFasL were added to transfected tumor cells at desired
333 E:T ratio/concentration, and incubated for 20 h at 37°C, 5% CO_2. For the viability setting, only
334 CLM was added to the tumor cells. After co-culture, supernatant was removed, remaining tumor
335 cells were lysed using 40 µL/well of cell lysis buffer for 10 min. After tumor cell lysis, 60 µL/well
336 of luciferase assay buffer was added and luciferase intensity was measured by using the Spark
337 20M plate reader (Tecan) with a counting time of 100 msec. Luciferase activities (relative

luminescence units = RLUs) were either represented as raw luciferase values or as normalized data to scramble or unstimulated controls.

Real-time live-cell imaging assay

Target genes in KMM-1 or U266 tumor cells were knocked down with reverse siRNA transfection for 48 h. The reverse siRNA transfection was performed using transparent 96 well microplates (TPP). In parallel, MILs were thawed and prepared as previously described in section MILs expansion. After 48 h, MILs (E:T 10:1) or rHuFasL (100 ng/mL) were added to the target cells in CLM with YOYO-1 (final concentration 1:5000) and co-cultured at 37°C. For viability controls, the according amount of CLM with YOYO-1 (final concentration 1:5000) was added. MILs or rHuFasL-mediated tumor lysis was imaged on the green channel using an IncuCyte ZOOM live cell imager (ESSEN BioScience) for the indicated time points at a 10x magnification. Data were analyzed with the Incucyte ZOOM 2016A software by creating a top-hat filter-based mask for the calculation of the area of YOYO-1 incorporating cells (indicating dead cells).

ELISA

Tumor cells were transfected with the indicated siRNAs (supplementary Table 2) in a 96-well plate. Afterwards, T cells were added at the indicated E:T ratio for 20 h and 100 µL of supernatants were harvested for the detection of IFN-γ (Human IFN-γ ELISA Set; BD OptEIA #555142), IL-2 (Human IL-2 ELISA Set; BD OptEIA #555190), Granzyme B (Human Granzyme B ELISA development kit; Mabtech #3485-1H-20) and TNF (Human TNF ELISA Set; BD OptEIA #555212). Experiments were performed according to the manufacturer´s instructions. Polyclonal stimulation (Dynabeads Human T-Activator CD3/CD28, Invitrogen #11131D) for 20 h was used

as positive control. Absorbance was measured at λ = 450 nm, taking λ = 570 nm as reference wavelength using the Spark microplate reader (TECAN).

Flow cytometry (FACS)

Flow cytometry was used for the detection of proteins expressed on the plasma membrane of tumor and T cells. Intracellular staining was performed for the detection of caspase-3 (FITC Active Caspase-3 Apoptosis Kit, BD Bioscience #550480) according to manufacturer's instruction. Tumor cells were detached from plates using PBS-EDTA, centrifuged at 500 x g for 5 min and resuspended in FACS buffer (5 x 10^5 cells/tube). Live T cell and tumor cells were distinguished by using Live/Dead Fixable Yellow dead Cell Stain (Thermo Scientific #L34959) according to manufacturer's instructions followed by blocking with kiovig (human plasma-derived immunoglobulin, Baxter, Deerfield, Illinois, USA) at a concentration of 100 µg/mL in FACS buffer (PBS, 2% FCS) for 15 min in the dark on ice. Samples were washed two times in FACS buffer and incubated with either fluorophore-conjugated primary antibodies or isotype control (APC anti-human CD274 (PD-L1) (Clone 29E.2A3), Biolegend #329707; Alexa Fluor 647 Mouse anti-human CCR9 (Clone 112509 (RUO), BD Biosciences #557975; Brilliant Violet 421 anti-human CD95 (Fas) (Clone DX2), Biolegend #305623; PE anti-human CD95 (Fas) (Clone DX2), BD Biosciences #555674; APC anti-human CD261 (DR4, TRAIL-R1) (Clone DJR1), Biolegend # 307207; PE anti-human CD262 (DR5, TRAIL-R2) (Clone DJR2), Biolegend # 307405; Biotin anti-human CD120a (TNFR1) (Clone W15099A), Biolegend #369908; PE/Cy7 anti-human CD120b (TNFR2) (Clone 3G7A02), Biolegend #358411; PE/Cy7 anti-human CD279 (PD-1) Antibody, Biolegend # 329918; APC mouse anti-human CD178 (Clone NOK-1), BD Biosciences #564262; PE anti-human CD253 (TRAIL) (Clone RIK2), Biolegend #308206; APC anti-human

384 TNF-α (Clone Mab11), Biolegend #502912 for 20 min on ice in the dark. Afterwards, cells were
385 washed twice, they were acquired with the FACS Canto II cell analyzer machine (BD Bioscience)
386 or FACSLyrics Flow cytometer, and data were analyzed using FlowJo (Tree Star).
387
388 **Calcium Imaging**
389 KMM-1 cells grown on coverslips were washed with Ringer solution (118 mM NaCl, 5 mM KCl,
390 1.2 mM MgCl2, 1.2 mM Na_2HPO_4, 2 mM NaH_2PO_4, 1.8 mM CaCl2, 5 mM glucose, 9.1 mM
391 HEPES, pH 7.4, with NaOH) and loaded with Fura-2-AM ester (Thermo Fisher Scientific,
392 Waltham, USA) for 45 min. After 15 min, MILs or rHuFasL (50 ng/ml) was added to scr siRNA
393 transfected cells and recording of the intracellular free Ca^{2+} was continued for further 30 minutes.
394 Experiments were performed using a ZEISS live cell imaging setup based on an inverse
395 microscope (Axio Observer Z.1) equipped with Fluar 40x/1.3 objective lens (ZEISS, Germany).
396 Fura 2-AM-loaded KMM-1 cells were illuminated with light of 340 nm or 380 nm (BP 340/30
397 HE, BP 387/15 HE) using a fast wavelength switching and excitation device (Lambda DG-4, Sutter
398 Instrument), and fluorescence was detected at 510 nm (BP 510/90 HE and FT 409) using an
399 AxioCam MRm LCD camera (ZEISS). Data were recorded and analyzed with ZEN 2012 software
400 (ZEISS, Jena, Germany).
401
402 **Generation of supernatants of activated MILs**
403 For the generation of the supernatant of polyclonally activated MILs, 1 x 10^6 MILs were suspended
404 in 1 mL of CLM collected in a 15 mL tube and stimulated with 25 µL of Dynabeads Human T-
405 Activator CD3/CD28 (Thermo Scientific) for 20 h. Afterwards, only the supernatant (100 µL/well)
406 of activated T cells was added to knocked down tumor cells and incubated overnight at 37°C, 5%

CO_2. Luciferase-based cytotoxicity assay was performed as described above. Alternatively, MILs were stimulated with tumor cells at an E:T ratio of 10:1. After 20 h co-culture, plates were centrifuged at 450 g for 5 min and 100 µL/well of the supernatant was collected for cytokines detection (ELISA).

Functional neutralization

For the functional neutralization experiment, anti-FasL (clone NOK-1, Biolegend #306409) or isotype control (Clone MOPC-21, Biolegend #400153) were pre-incubated with MILs for 1 h at 37°C, 5% CO_2. As negative control, antibodies were cultivated in the absence of T cells. Afterwards, antibody-containing supernatants were used to stimulate KMM-1-luc cells, which were reverse transfected with the indicated siRNAs (supplementary Table 2). The final concentration of the neutralizing antibodies was 100 ng/mL for anti-FasL and isotype control. As positive control recombinant FasL protein (100 ng/ml, Biolegend #589404) was added to the tumor cells instead of T cells. 20 h after co-culture, luciferase intensity was measured as described above.

Blocking assays

For the experiments using the anti-Calmodulin (W-7 hydrochloride) (Tocris #0369) inhibitor, 1 x 10^4 KMM-1-luc (scr or CAMK1D-transfected) cells/well were seeded in white 96 well plates (Perkin Elmer) in 100 µL of RPMI 10 % FCS. The small molecule inhibitor was added at the indicated concentrations for 1 h at 37°C, before 100 ng/mL rHuFasL or medium control was added. DMSO treatment served as negative control. After 20 h stimulation, luciferase-based cytotoxicity assay was performed. For CAMK1D inhibition, 1 x 10^4 KMM-1-luc or 1 x 10^4 Mel270 cells/well were incubated overnight in a 96 well plate. QPP-A inhibitor (Merck Millipore; CAS 404828-08-

6) was added at the indicated concentrations 1h before rHuFasL stimulation (100 ng/ml) or medium control. DMSO treatment served as negative control. After 20h stimulation, luciferase-based cytotoxicity assay was performed.

Luminex assays

Tumor cells were stimulated with rHuFasL (100 ng/mL) for 15 min, 30 min, 1 h, 2 h, 4 h and 8 h. Unstimulated cells served as controls. For the detection of intracellular phosphorylated analytes, a general pathway (MILLIPLEX MAP Multi-Pathway Magnetic Bead 9-Plex kit, Merck Millipore #48-680MAG) was used following manufacturer's instructions. For the detection of proteins involved in the activation of apoptosis the MILLIPLEX MAP Early Phase Apoptosis 7-plex-kit (Merck Millipore #48-669MAG) together with active caspase-3 Magnetic Bead MAPmate (Merck Millipore #46-604MAG) were used following manufacturer's instructions. Beads specific for GAPDH (MILLIPLEX MAP GAPDH Total Magnetic Bead MAPmate) (Merck Millipore #46-667MAG) served as normalization control. 20 µg of protein lysates were used for the detection of ERK/MAP kinase 1/2 (Thr185/Tyr187), Akt (Ser473), STAT3 (Ser727), JNK (Thr183/Tyr185), p70 S6 kinase (Thr412), NF-kB (Ser536), STAT5A/B (Tyr694/699), CREB (Ser133), and p38 (Thr180/Tyr182) phosphorylated Akt (Ser473), JNK (Thr183/Tyr185), Bad (Ser112), Bcl-2 (Ser70), p53 (Ser46), cleaved caspase-8 (Asp384), cleaved caspase-9 (Asp315) and active caspase-3 (Asp175). The assay was performed according to the manufacturer´s instructions and samples were measured using the MAGPIX Luminex instrument (Merck Millipore).

High-throughput RNAi screening

Primary RNAi screening

453 The primary RNAi screening was conducted using a sub-library of the genome-wide siRNA library
454 siGENOME (Dhamacon, GE healthcare), which comprised 2887 genes (1288 genes for
455 GPCR/kinase and 1599 genes for custom library). The library was prepared in Prof. Boutros´s
456 group (DKFZ, Heidelberg) as described in (48). Each well contained a pool of four non-
457 overlapping siRNAs (SMARTpool) targeting the same gene. This arrayed screening approach was
458 performed in duplicates and was adopted from Khandelwal et al (49). The siRNA sequences of the
459 genome-wide library were distributed in the 384-well plates and positive and negative siRNA
460 controls were added in empty wells. The final concentration of all siRNA sequences was 25 nM.
461 Reverse transfection was performed as described in section reverse siRNA transfection. The read-
462 out was performed using Mithras LB 940 microplate Reader with a counting time of 100 msec. 40
463 x 384-well plates were subjected to the luciferase-based screening assay performed on KMM-1-
464 luc cells. 20 x 384-well plates were subjected to the luciferase-independent CellTiter-Glo (CTG)
465 screening performed on luciferase-negative KMM-1 cells without the addition of MILs in order to
466 exclude genes affecting cell viability. Briefly, for the read-out, supernatant was removed in each
467 well containing siRNA-transfected tumor cells and 20 μL of the CTG reagent (pre-diluted 1:4 in
468 RPMI) were added. After 15 min incubation in the dark, plates were measured using the Mithras
469 reader as described above.
470 For the screening analysis, the raw RLUs from the primary screening were processed using the
471 cellHTS2 package in R/Bioconductor (50). Values from both conditions were quantile normalized
472 against each other using the aroma.light package in R. Pearson correlation (r^2) between the two
473 replicate values was calculated for each setting. Differential scores (cytotoxicity vs. viability) were
474 calculated using the LOESS local regression method. To identify candidate hits, the following
475 thresholds were applied on the z-scores of the samples: for the viability setting, genes showing a z

> + 2,0 or z < - 2,0 were excluded. For the cytotoxicity setting, CCR9 was used as threshold score. Additionally, genes having a z-score > + 0,5 or < - 0,5 in the CTG-based viability screening were filtered out from the candidate list.

Secondary screening

For the secondary screening, a customized library (G-CUSTOM-223794) containing 128 genes from the primary screening was distributed in several 96-well plates along with positive and negative siRNA controls. Reverse transfection was performed. For the cytotoxicity setting MILs (10:1 ratio) or supernatant of anti-CD3/anti-CD28 magnetic beads activated MILs were added to knockdown tumor cells (1 x 10^4 cells/well). Instead, CLM medium was added to the viability plates. After 20 h, luciferase-based read-out was performed. RLUs were normalized to Mock control. Cytotoxicity/viability ratios were calculated according to the formula: Cytotoxicity/viability ratio = (Norm. RLU cytotoxicity setting / Norm. RLU viability setting). The hit-list was generated by including only hits with improved T cell-mediated cytotoxicity over mock transfection, (Cytotoxicity/viability ratio < 1). Pearson´s correlation was calculated with Microsoft Excel.

***In vivo* experiments**

Camk1d knockout MC38 murine colorectal cells were generated using the CRISPR/Cas9 technique. In vivo experiments were performed in two cohorts of mice: C57BL6 (n=12) and NOD/SCID gamma chain (NSG) mice (n=12) were subcutaneously injected with 1 x 10^5 MC38 Camk1d KO (g3 clone 11) or 1 x 10^5 MC38 NTS (clone 12) cells each into the right and left flank of one mouse, respectively. Tumor growth was measured twice a week with a caliper and the

volume was determined using the following formula: Tumor volume (mm^3) = ($Width^2$ x Length) x (π / 6). Mice were sacrificed when tumors exceeded 1.5cm in diameter.

Statistics

For statistical analysis, GraphPad Prism software v6.0 (GraphPad Software, La Jolla, CA, USA was used. If not stated, statistical differences between the control and the test groups were determined by using two-tailed unpaired Student's t-test. In all statistical tests, a p-value ≤ 0.05 was considered significant with * = $p \leq 0.05$, ** = $p \leq 0.01$, *** = $p \leq 0.001$ and **** = $p \leq 0.0001$.

Results

MM cells expressed multiple genes that confer intrinsic resistance towards T cell attack

In order to identify novel genes involved in immune escape mechanisms of PD-L1 unresponsive cancer cells, a high-throughput (HTP) screening approach (49) was adapted. The HLA-A2 positive human multiple myeloma (MM) cell line KMM-1, expressing high levels of PD-L1 and lower levels of CCR9 (49), was used as a tumor model in this study. As a reporter system for tumor cell survival, we stably transfected KMM-1 cells with e-GFP-firefly luciferase, allowing for luminescence imaging to detect immune-mediated tumor cell destruction in a HTP format (Figure 1A).

As a source of tumor-reactive T cells we used marrow-infiltrating, PD-1 positive T cells (MILs) from an HLA-A2-matched patient (Figure 1A and Supplementary Figure S1A). These MILs were not terminally exhausted as they displayed strong IFN-gamma secretion after polyclonal stimulation (Figure 1B), which exceeded that of tumor antigen specific $CD8^+$ cytotoxic Survivin T cells (49). MILs recognized KMM-1 tumor cells, despite high PD-L1 expression (Figure 1B).

However, their limited killing capacity (Supplementary Figure S1B) suggested the presence of resistance mechanisms against T cell induced death.

Silencing of firefly-luciferase (siFLuc), ubiquitin C (UBC), a gene essential for cell survival, or transfection with a mixture of siRNAs inducing cell death (siCD) resulted in strong reduction of luciferase expression, indicating appropriate gene silencing and sensitivity of the luciferase-based readout. This was also maintained upon co-culture of siRNA treated KMM-1 cells with MILs (Figure 1C).

We next studied the effect of PD-L1 and CCR9 on KMM-1 cells (Figure 1D). The knockdown of PD-L1 did not result in increased KMM-1 killing by MILs, despite high expression of PD-L1 on the tumors and of PD-1 on the MILs (Figure 1E). In contrast, CCR9 silencing significantly improved tumor cell rejection (Figure 1E), suggesting that PD-L1 did not play a decisive role in immune resistance of KMM-1 cells. We therefore used CCR9 as positive control within the screen.

To this end, KMM-1 cells were transfected in a multi-well format with a siRNA library consisting of a pool of four non-overlapping siRNAs per target per well, targeting a total of 2887 genes (supplementary Table 1) covering a broad spectrum of all gene families. The screening approach comprised a viability setup, in which we assessed the intrinsic viability effect of each gene knockdown, and a cytotoxicity setup, where siRNA transfected tumor cells were co-cultured with MILs (Supplementary Figure S2).

Negative (scramble siRNA sequences, scr1 and scr2) and positive controls (siRNAs-targeting luciferase and essential viability genes) were included as a reference to calculate the effect of gene knockdown on cell viability. Overall, the distribution of values across test replicates and setups was highly concordant showing no viability or cytotoxicity effect of scr siRNAs but robust signal reduction after FLuc and UBC knockdown (Figure 2A). Calculated z-scores for the impact on cell

545 viability and T cell cytotoxicity (Figure 2B) and for the relative impact on T cell-mediated tumor
546 cell lysis (Loess score) of each gene, revealed 128 genes whose silencing improved tumor cell
547 lysis by T cells to a higher degree than CCR9 (Figure 2C). Among them we found several genes
548 with described immune regulatory function in MM such as *CD5* (51), *FES* (52) and *PAK3* (53).
549 PD-L1 did not have any effect on T cell-mediated killing of MM cells (Figure 2B, C). The
550 identification of these validated immune-checkpoints in combination with good immune-
551 checkpoint control performance supported the robustness and sensitivity of the screen.
552 For further validation, we subjected the 128 candidate hits to a secondary screening procedure
553 using the same setup as for the HTP screen. Silencing of 90 candidates again increased T cell-
554 mediated killing of tumor cells, and only had little effect on intrinsic tumor cell viability, thus
555 confirming their immune regulatory role in KMM-1 cells (Figure 2D). The highest immune
556 modulatory effect was elicited by the serine/threonine calcium/calmodulin-dependent protein
557 kinase 1D (CAMK1D) (Figure 2B-D).
558 To determine whether the observed tumor cell killing was mediated by cytokines or other soluble
559 proteins released by activated MILs, an additional setting was included. MILs were polyclonally
560 stimulated with anti-CD3/anti-CD28 magnetic beads and only their cell culture supernatant was
561 added to the tumor cells. In this setup, silencing of few genes had an impact on tumor cell lysis
562 indicating a role in resistance towards T-cell secreted cytotoxic cytokines (Figure 2E). Most of the
563 identified candidate genes, including CAMK1D, regulated tumor cell killing only upon direct
564 interaction with T cells. Taken together, these results provided an indication that MM cells express
565 multiple immune regulatory genes, among them CAMK1D, that confer immune resistance after T
566 cell engagement.
567

CAMK1D protected PD-L1$^+$ tumor cells against death receptor signaling by cytotoxic T cells

Based on the immune resistance phenotype associated with CAMK1D expression in our screens, we validated and characterized the immune regulatory role of CAMK1D. We first de-convoluted the pool of siCAMK1D to exclude potential dominant off-target effects of single siRNAs within the pool. Three out of four siRNAs (s1, s2 and s3) and the pool of all siRNAs increased T cell-mediated cytotoxicity, whereas no viability impact was detected (Figure 3A). All siRNAs significantly reduced CAMK1D mRNA and protein expression (Figure 3B, C). In a luciferase-independent assay, employing live cell-imaging, we confirmed an increase MIL-induced apoptosis of CAMK1D-deficient KMM-1 cells (Figure 3D). This could be inhibited with MHC-I blocking antibodies, indicating that tumor cell apoptosis was induced by MHC-I-restricted CD8$^+$ MILs in a T cell receptor-dependent manner (Figure 3E). To corroborate this finding, we pulsed KMM-1 cells with an HLA-A2-restricted influenza (flu) peptide and co-cultured them with PD-1 positive, flu-peptide-specific CD8$^+$ cytotoxic T cells (flu TC) (Supplementary Figure S3A). Again, siCAMK1D, but not PD-L1 silencing, resulted in a significant increase of T cell-mediated tumor cell lysis (Figure 3F and Supplementary Figure S3B). These data demonstrated that CAMK1D mediated resistance of KMM-1 cells towards antigen-specific T cells, independent of the T cell source. CAMK1D-mediated immune protection also occurred in the PD-L1$^+$, HLA-A2$^+$ MM cell line, U266 (Figure 3G-I and Supplementary Figure S3C). We therefore studied CAMK1D expression in a large cohort of CD138-purfied malignant plasma cells from MM patients with monoclonal gammopathy of unknown significance (MGUS), human myeloma cell lines (HMCL), memory B cells (MBC), plasmablasts (PPC) and normal bone marrow plasma cells (BMPC). CAMK1D expression was highest in MBC, but was also expressed in all MM, MGUS, PPC, and in 30/32 HMCL samples, with higher expression than normal bone marrow plasma cells (BMPCs)

(Figure 3J). Thus, these data indicated that CAMK1D was consistently expressed in human multiple myelomas and conferred resistance against cytotoxic T cell attack.

As classical immune-checkpoint molecules expressed by tumor cells regulate T cell activity mostly through engagement of inhibitory receptors (54), we wondered whether CAMK1D, being an intracellular kinase, might indirectly regulate T cell activity. We therefore studied parameters of T cell effector function upon contact with CAMK1D-proficient or -deficient KMM-1 cells, including the secretion of INF-γ, Granzyme B, IL-2, or TNF-α.

Although we consistently detected increased T cell-mediated tumor cell killing after CAMK1D knockdown in KMM-1 cells, functional analysis of T cells did not reveal any increased T cell function after interaction with CAMK1D-deficient compared to wt tumor cells (Supplementary Figure S3D). Therefore, we concluded that CAMK1D did not affect type 1 effector T cell function and hypothesized that it may instead have regulated the sensitivity of tumor cells towards cytotoxic T cell attack. Thus, we exposed KMM-1 cells to the cytotoxic agents FasL (rHuFasL), TRAIL (rHuTRAIL) or TNF (rHuTNF) commonly used by T cells to kill their target cells. The respective cell death-mediating receptors for FasL and TRAIL, Fas, DR4 and DR5 were highly expressed on KMM-1 cells while the TNF receptors TNFR1 and TNFR2 were not (Figure 4A). Whereas CAMK1D-proficient KMM-1 cells were resistant against all tested cytotoxic agents, CAMK1D-deficient tumor cells were dramatically reduced after exposure to FasL and TRAIL (Figure 4B). We also detected FasL on 28.2% and 16.1% of $CD4^+$ and $CD8^+$ MILs, respectively (Figure 4C) and on 12.7% of flu TC (Supplementary Figure S3E). TRAIL expression was detected only on 12.5% and 5.3% of $CD4^+$ and $CD8^+$ MILs, while membrane bound TNF was hardly detectable (Figure 4C). Neutralization of FasL by monoclonal antibodies completely abrogated CAMK1D-induced protection against the cytotoxic activity of MILs (Figure 4D). Thus, CAMK1D mediated

intrinsic tumor resistance against activated T cells by interfering with Fas-mediated death signaling. In line with this, U266 cells highly expressed Fas (Figure 4E) and were protected by CAMK1D expression against Fas-mediated cell death similar to KMM-1 cells (Figure 4F).

Since Fas-FasL interactions represent a major cytotoxic mechanism, we tested if CAMK1D protected also solid tumors against immune rejection. In the human cancer cell lines PANC-1 and MCF7, Fas expression was low. However, we found high Fas and CAMK1D expression in Mel270, a PD-L1^{+} human uveal melanoma (UVM) cell line (Figure 4G, H and Supplementary Figure S4A). UVM is a highly treatment-refractory and anti-PD-1-resistant subtype of melanoma (55). Silencing of CAMK1D significantly increased the cytolytic response of Mel270 towards FasL exposure (Figure 4I), indicating that uveal melanomas exploited CAMK1D for resistance against T cell-attack. In contrast, CAMK1D silencing in the Fas negative tumor cell lines PANC-1 and MCF-7 did not sensitize these cells towards T cell-killing (Supplementary Figure S4B and 4C). These data provided rationale for CAMK1D inhibition only in the context of Fas-positive tumors to achieve significant antitumor immune response. We hypothesized that CAMK1D expression in UVM might protect those tumors with strong Fas expression against immune rejection. We therefore stratified patients in the TCGA database cohort according to CAMK1D and Fas. Kaplan-Meier analyses showed that overexpression of CAMK1D in Fas receptor^{high} but not in Fas receptor^{low} tumors correlated with poor patient prognosis (Figure 4J). This suggested that CAMK1D exerted a tumor protective effect only in the context of Fas activation during an immune response. Overexpression of CAMK1D and PD-L1 were tightly co-regulated in uveal melanomas (Figure 4K). Consequently, our study with PD-L1 expressing yet refractory tumor models shows that CAMK1D represented another level of immune resistance superseding the PD-L1 axis in mediating immune-suppression.

637 Using the TCGA database we studied CAMK1D and PD-L1 co-regulation in other tumor entities
638 that are largely unresponsive to anti-PD-1 treatment, specifically ovarian, stomach and esophageal
639 carcinomas (56, 57). As observed in UVM, CAMK1D and PD-L1 were co-expressed and we
640 detected significant correlations of CAMK1D and Fas receptor expression with poor outcomes
641 (Supplementary Figure S5A-F). Hence, CAMK1D is co-regulated with PD-L1 and controls tumor
642 rejection after Fas receptor activation in several anti-PD-1 treatment refractory tumors.

643

644 **CAMK1D regulated the activity of effector caspases -3, -6 and -7 after Fas activation**

645 FasL binding to Fas receptor results in complex signaling events leading to a caspase cascade that
646 initiates apoptosis (58); this binding also stimulates Ca^{2+} influx into the cytoplasm, which
647 ultimately triggers CAMK1D activation (59). We speculated that CAMK1D might interfere with
648 the apoptotic cascade to mediate its tumor protective effect. Thus, we assessed the impact of
649 CAMK1D expression on tumor cell killing in the absence of effector caspases. Silencing of each
650 downstream effector caspase -3, -6 and -7 completely abrogated the increased lysis of CAMK1D-
651 deficient tumor cells after FasL exposure (Figure 5A, B). Thus, CAMK1D selectively regulated
652 cellular sensitivity towards apoptotic cell death. These results demonstrated the necessity of
653 simultaneous activity of all three effector caspases for efficient induction of apoptotic cell death
654 after Fas activation.

655 CAMK1D activation depends on Ca^{2+}/calmodulin (CaM) binding, allowing the CAMK-kinase
656 (CAMKK) to phosphorylate and fully activate CAMK1D (59, 60). We speculated that FasL-
657 expressing MILs might trigger Ca^{2+} release and therefore compared intracellular Ca^{2+} in KMM-1
658 cells on single cell level after exposure to MILs or rHuFasL. Shortly after treatment both conditions
659 induced an increase of intracellular Ca^{2+} (Figure 5C, D).

W-7 hydrochloride inhibits Ca^{2+}/calmodulin complexes (61) consequently impacting CAMK1D activation. Treatment with 5µM W-7 hydrochloride was not toxic to KMM-1 cells (Figure 5E) and sharply recapitulated the effect of CAMK1D silencing on FasL induced tumor cell apoptosis, suggesting that CAMK1D was the decisive target of calmodulin for mediating FasL resistance (Figure 5F). Since both CAMK1D silencing and W-7 hydrochloride treatment only incompletely blocked CAMK1D, we explored whether their combination reduced cell viability after FasL exposure. This combinatorial treatment resulted in a 3-fold further increase of tumor cell killing (Figure 5F). To corroborate these findings, we applied CAMK1D-inhibitor (QPP-A) to MM and UVM cell lines. The additional treatment with rHuFasL induced a significant loss of tumor cell viability, confirming that CAMK1D played a substantial role in conferring resistance towards apoptosis (Figure 5G).

These results demonstrated that CAMK1D activation in cancer cells was (i) triggered by CTL via FasL-induced Ca^{2+} release and (ii) was required to control Fas-induced tumor cell apoptosis. To confirm the immune-resistant role of CAMK1D *in vivo*, we knocked out Camk1d in the murine colorectal cell line MC38 (Supplementary Figure S6A). *In vitro* analysis of Camk1d-deficient tumor cells revealed their increased sensitivity towards FasL as well as TRAIL-mediated apoptosis (Supplementary Figure S6B). Thus, we injected MC38 -Camk1d KO and -NTS (non-targeting sequence) cells into the left and right flank of the same mouse of both immunodeficient NSG and immunocompetent C57BL6 mice. Camk1d KO and NTS tumors developed rapidly in a similar manner in NSG mice, whereas a significant difference was observed in C57BL6 mice where Camk1d-deficient tumors were significantly reduced (Figure 5H). These data demonstrated that the immune system in immunocompetent mice was not able to reduce tumor outgrowth due to Camk1d expression.

To elucidate CAMK1D involvement in the Fas-signaling cascade, we studied activation of caspase-8 and -9, the prototypic initiator caspases of the extrinsic and intrinsic apoptotic pathway, respectively (62). FasL-induced activation of both caspases was comparably effective in CAMK1D-proficient and -deficient KMM-1 cells (Figure 6A, B). Consequently, we hypothesized that CAMK1D regulated the activity of downstream effector caspases. To this end, we first studied the activation of the central executioner caspase-3. We observed an increase in caspase-3 activation in CAMK1D-deficient KMM-1 cells after FasL treatment (Figure 6C-E). In addition, we also detected increased cleavage of the effector caspases -6 and -7 in CAMK1D-deficient tumor cells (Figure 6F and Supplementary Figure S7A). The phosphorylation and activation of the transcription factor cAMP response element-binding protein (CREB) was increased in CAMK1D-proficient cells, which was responsible for the transcription of the anti-apoptotic molecule Bcl-2 (Supplementary Figure S7B). We also observed that at early time-points (15min, 30min and 1h) after rHuFasL stimulation, the phosphorylation of Extracellular Signal-regulated Kinases (ERK1/2) was enhanced in wild-type cells, but not in CAMK1D knockdown cells (Supplementary Figure S7B). The altered activation of the presented proteins implied that CAMK1D not only controlled activation and activity of effector caspases but also induced the expression of anti-apoptotic and mitogenic proteins leading to tumor cell resistance towards FasL-positive T cells. CAMK1D has thus far not been established as a regulator of effector caspase activity. In silico analysis predicted a binding motif for CAMK1D on caspase-3 and caspase-6 (Supplementary Figure S7D). Notably, CAMK1D co-immunoprecipitated with caspase-3, caspase-6 and caspase-7 and the interaction increased upon rHuFasL treatment (Figure 6G, H and Supplementary Figure S7C). A direct CAMK1D/effector caspase interaction could result in stoichiometric inhibition of caspase cleavage by initiator caspases. Alternatively, the effector caspases may also serve as

706 targets of CAMK1D kinase activity. Phosphorylation of inhibitory serine residues impedes
707 caspases activation, proteolytic activity and ultimately hampers apoptosis induction (63).
708 The inhibitory phosphorylation sites of caspase-3 (Ser150) and caspase-6 (Ser257) (64, 65) were
709 located in the kinase-function critical distance of up to 4 amino acids apart from the predicted
710 binding site for CAMK1D (Supplementary Figure S7D). We therefore wondered whether
711 CAMK1D was able to phosphorylate Ser150 and Ser257 of caspase-3 and -6, respectively.
712 CAMK1D deficient KMM-1 cells had reduced phosphorylation of inhibitory serine residues on
713 both caspase-3 and -6 already at steady–state conditions (Figure 6I-L). In KMM-1 wt cells,
714 phosphorylation transiently decreased 15min - 30min after FasL treatment (which is attributed to
715 transient stimulation of phosphatases (66)), but recovered to pre-stimulation expression within 1h
716 (caspase-3) to 4h (caspase-6). In contrast, caspase-3 and -6 phosphorylation was persistently low
717 in CAMK1D-deficient KMM-1 cells, resulting in overall much lower caspase inactivation
718 compared to CAMK1D wt cells. This demonstrated that CAMK1D was required for steady-state
719 inactivation of effector caspases through phosphorylation and for the rapid restoration of caspase-
720 3 and -6 phosphorylation after FasL stimulation.
721 CAMK1D, upon its activation through FasL, regulated activation and activity of all effector
722 caspases after cytotoxic T cell encounter. These results suggested that this effect was at least
723 partially achieved by the inhibitory phosphorylation of the effector caspases.
724

725 **Discussion**

726 Despite noteworthy improvements in the field of immunotherapy, where immune-checkpoint
727 blockade (ICB) has broad clinical success (11, 13, 14, 67) a significant proportion of cancer
728 patients do not respond to ICB (15, 16, 68). Unknown immune-checkpoint molecules might be

729 employed by tumor cells to escape the antitumor immune response. Here, we used a multiple
730 myeloma cell line to conduct a systematic search for genes controlling immune rejection in PD-
731 L1 refractory human tumors. Among the identified genes, CAMK1D was chosen for further
732 validation and mode of action analysis. CAMK1D expression is elevated in invasive carcinomas
733 compared to carcinoma in situ and overexpression of CAMK1D in non-tumorigenic breast
734 epithelial cells increased proliferation and epithelial-mesenchymal transition (69). We reported a
735 different role of CAMK1D in controlling the resistance of PD-L1^{+} tumor cells against apoptosis
736 triggered by cytotoxic T cells. Tumor cell killing in CAMK1D-deficient cells was independent of
737 the T cell source, as both MILs and flu-specific CD8^{+} T cells were able to reproduce the same
738 effect. Tumor cells can evade the immune system either by intrinsically increasing tumor cell
739 resistance (70) or by hampering immune cell activation (54). Our data demonstrated that
740 CAMK1D-deficient tumor cells did not enhance T cell function. On the other hand, CAMK1D
741 acted as central mediator of intrinsic tumor resistance towards CTL. Cytotoxic T cells eliminate
742 tumor cells through the extrinsic apoptosis pathway, initiated by death receptors signaling,
743 activating pro-caspase-8 (58, 71, 72), or by triggering the intrinsic pathway through the release of
744 cytotoxic granules. This induces mitochondrial damage, apoptosome formation and subsequent
745 activation of pro-caspase-9 (73). Both initiator caspases activate the common executioner caspases
746 -3, -6 and -7, which in turn cleave key intracellular substrates including endonucleases, thus
747 irreversibly triggering the apoptotic cell death (74, 75). We observed that the initiator caspases -8
748 and -9 were not differentially affected in CAMK1D-proficient and -deficient tumor cells. Caspase-
749 8 is inactivated upon phosphorylation of tyrosine-380, which leads to increased resistance to
750 CD95-induced apoptosis (76). However, CAMK1D is a serine/threonine protein kinase and in
751 silico analysis revealed no binding site between CAMK1D and Caspase-8. Co-expression of death

752 receptor ligands and cytotoxic granules enabled CTL to simultaneously trigger both apoptosis
753 pathways, which differed from other common mechanisms of cell apoptosis which generally
754 trigger either one or the other pathway (77). Therefore, efficient resistance mechanisms against T
755 cell-induced apoptosis may target the common end route of both pathways. Consequently,
756 inhibition of effector caspase activity may represent a hallmark of tumor immune resistance.
757 Caspases can be regulated by post-translational modifications such as phosphorylation and
758 ubiquitylation that can block caspases activation and activity (63). Indeed, phosphorylation of
759 caspase-3 by p38 at Ser150, directly inhibits caspase-3, hindering Fas-induced apoptosis in
760 neutrophils (64). Likewise, in the colon cancer cell line SW480, caspase-6 is inhibited by ARK5-
761 phosphorylation, leading to the evasion of Fas-induced apoptosis (65). Caspase-7 can be inhibited
762 post-translationally by PAK2-medited phosphorylation at Ser30, Thr173 and Ser239, which
763 negatively regulates caspase-7 activity (78). We proposed a model where FasL stimulation
764 increases calcium release from the ER, thereby binding and activating calmodulin, the upstream
765 activator of CAMK1D. The binding of calmodulin to CAMK1D allows CAMKK to phosphorylate
766 and fully activate CAMK1D. As a consequence, CAMK1D bound to the effector caspases
767 inhibiting their activation acting as a direct stoichiometric inhibitor and by phosphorylation
768 CAMK1D subsequently reduced the activity of the effector caspases. Moreover, activated
769 CAMK1D translocated into the nucleus where it phosphorylated and activated CREB, leading to
770 the transcription of Bcl-2. Thus, CAMK1D is an immune-checkpoint molecule that interferes with
771 tumor cell death, sustaining anti-apoptotic pathways.
772 As CAMK1D is ubiquitously expressed, the pharmacological inhibition may increase tumor
773 susceptibility towards T cell attack, but also impair T cell activity. In line with this concern,
774 blockade of the tyrosine kinase JAK2 sensitized MM tumor cells to NK cell attack (79); however,

775 the function of NK and T cells was impaired in human myeloproliferative neoplasms (80-82).
776 More studies must be conducted to clarify the impact of CAMK1D targeted therapy on T cells.
777 Nonetheless, CAMK1D remains a potential target for cancer immunotherapy, in particular for
778 those patients who experience relapse or demonstrate unresponsiveness to conventional therapies.
779 Our studies confirm the role of CAMK1D *in vivo* as a novel immune-checkpoint molecule
780 conferring resistance towards immune attack. It is conceivable that tumor cells exploit Fas
781 signaling imposed by cytotoxic T cells to activate an apoptosis resistance mechanism targeting the
782 final effector expression of both intrinsic and extrinsic apoptotic pathways resulting in an increased
783 resistance to immune cell attack. In T cell-infiltrated tumors, this mechanism may impact the
784 treatment resistance of tumor cells, as CAMK1D may reduce the efficacy of antitumor treatments
785 that directly or indirectly exploit the intrinsic apoptotic signaling pathways to trigger cancer cell
786 death.

787

788 **Author contributions**: VV, TM, AS, ANM, GK, MD, VMM, CYC and ASz performed
789 experiments and VV and TM conducted bioinformatics analyses. VV, TM, AS and PB designed,
790 conducted and analyzed the HTP screen. VV and PB designed the study and drafted the
791 manuscript. All authors contributed to the manuscript preparation.
792
793 **Acknowledgments**: We thank Dr. Haase (LMU, Munich) for the pEGFP-Luc plasmid, Prof.
794 Moldenhauer (DKFZ, Heidelberg) for the MHC-I antibody and Martins Freire (iOmx Therapeutics
795 AG, Martinsried) for the bulk MC38-Camk1d knockout cells.

796 This work was supported by the Deutsche Forschungsgemeinschaft (DFG, German Research
797 Foundation) - Projektnummer 324392634 - TRR 221 and the National Research, Development and
798 Innovation Office, Hungary - OTKA K119690.
799

References

1. Choi C, Witzens M, Bucur M, Feuerer M, Sommerfeldt N, Trojan A, Ho A, Schirrmacher V, Goldschmidt H, and Beckhove P. Enrichment of functional CD8 memory T cells specific for MUC1 in bone marrow of patients with multiple myeloma. *Blood.* 2005;105(5):2132-4.
2. Safi S, Yamauchi Y, Rathinasamy A, Stamova S, Eichhorn M, Warth A, Rauch G, Dienemann H, Hoffmann H, and Beckhove P. Functional T cells targeting tumor-associated antigens are predictive for recurrence-free survival of patients with radically operated non-small cell lung cancer. *Oncoimmunology.* 2017;6(11):e1360458.
3. Schmitz-Winnenthal FH, Volk C, Z'Graggen K, Galindo L, Nummer D, Ziouta Y, Bucur M, Weitz J, Schirrmacher V, Buchler MW, et al. High frequencies of functional tumor-reactive T cells in bone marrow and blood of pancreatic cancer patients. *Cancer research.* 2005;65(21):10079-87.
4. Galon J, Costes A, Sanchez-Cabo F, Kirilovsky A, Mlecnik B, Lagorce-Pages C, Tosolini M, Camus M, Berger A, Wind P, et al. Type, density, and location of immune cells within human colorectal tumors predict clinical outcome. *Science.* 2006;313(5795):1960-4.
5. Reissfelder C, Stamova S, Gossmann C, Braun M, Bonertz A, Walliczek U, Grimm M, Rahbari NN, Koch M, Saadati M, et al. Tumor-specific cytotoxic T lymphocyte activity determines colorectal cancer patient prognosis. *J Clin Invest.* 2015;125(2):739-51.
6. Pardoll DM. The blockade of immune checkpoints in cancer immunotherapy. *Nat Rev Cancer.* 2012;12(4):252-64.
7. Abiko K, Matsumura N, Hamanishi J, Horikawa N, Murakami R, Yamaguchi K, Yoshioka Y, Baba T, Konishi I, and Mandai M. IFN-gamma from lymphocytes induces PD-L1 expression and promotes progression of ovarian cancer. *British journal of cancer.* 2015;112(9):1501-9.
8. Alsaab HO, Sau S, Alzhrani R, Tatiparti K, Bhise K, Kashaw SK, and Iyer AK. PD-1 and PD-L1 Checkpoint Signaling Inhibition for Cancer Immunotherapy: Mechanism, Combinations, and Clinical Outcome. *Frontiers in pharmacology.* 2017;8(561.
9. Zou W, Wolchok JD, and Chen L. PD-L1 (B7-H1) and PD-1 pathway blockade for cancer therapy: Mechanisms, response biomarkers, and combinations. *Sci Transl Med.* 2016;8(328):328rv4.
10. Yokosuka T, Takamatsu M, Kobayashi-Imanishi W, Hashimoto-Tane A, Azuma M, and Saito T. Programmed cell death 1 forms negative costimulatory microclusters that directly inhibit T cell receptor signaling by recruiting phosphatase SHP2. *J Exp Med.* 2012;209(6):1201-17.
11. Hodi FS, O'Day SJ, McDermott DF, Weber RW, Sosman JA, Haanen JB, Gonzalez R, Robert C, Schadendorf D, Hassel JC, et al. Improved survival with ipilimumab in patients with metastatic melanoma. *N Engl J Med.* 2010;363(8):711-23.
12. Slovin SF, Higano CS, Hamid O, Tejwani S, Harzstark A, Alumkal JJ, Scher HI, Chin K, Gagnier P, McHenry MB, et al. Ipilimumab alone or in combination with radiotherapy in metastatic castration-resistant prostate cancer: results from an open-label, multicenter phase I/II study. *Ann Oncol.* 2013;24(7):1813-21.
13. Yang JC, Hughes M, Kammula U, Royal R, Sherry RM, Topalian SL, Suri KB, Levy C, Allen T, Mavroukakis S, et al. Ipilimumab (anti-CTLA4 antibody) causes regression of metastatic renal cell cancer associated with enteritis and hypophysitis. *Journal of immunotherapy.* 2007;30(8):825-30.
14. Topalian SL, Hodi FS, Brahmer JR, Gettinger SN, Smith DC, McDermott DF, Powderly JD, Carvajal RD, Sosman JA, Atkins MB, et al. Safety, activity, and immune correlates of anti-PD-1 antibody in cancer. *N Engl J Med.* 2012;366(26):2443-54.
15. Bu X, Mahoney KM, and Freeman GJ. Learning from PD-1 Resistance: New Combination Strategies. *Trends Mol Med.* 2016;22(6):448-51.
16. Carbognin L, Pilotto S, Milella M, Vaccaro V, Brunelli M, Calio A, Cuppone F, Sperduti I, Giannarelli D, Chilosi M, et al. Differential Activity of Nivolumab, Pembrolizumab and MPDL3280A according to the Tumor Expression of Programmed Death-Ligand-1 (PD-L1): Sensitivity Analysis of Trials in Melanoma, Lung and Genitourinary Cancers. *PLoS One.* 2015;10(6):e0130142.
17. Hugo W, Zaretsky JM, Sun L, Song C, Moreno BH, Hu-Lieskovan S, Berent-Maoz B, Pang J, Chmielowski B, Cherry G, et al. Genomic and Transcriptomic Features of Response to Anti-PD-1 Therapy in Metastatic Melanoma. *Cell.* 2016;165(1):35-44.
18. Nowicki TS, Hu-Lieskovan S, and Ribas A. Mechanisms of Resistance to PD-1 and PD-L1 Blockade. *Cancer journal.* 2018;24(1):47-53.

19. Fourcade J, Sun Z, Benallaoua M, Guillaume P, Luescher IF, Sander C, Kirkwood JM, Kuchroo V, and Zarour HM. Upregulation of Tim-3 and PD-1 expression is associated with tumor antigen-specific CD8+ T cell dysfunction in melanoma patients. *J Exp Med.* 2010;207(10):2175-86.
20. Wang L, Rubinstein R, Lines JL, Wasiuk A, Ahonen C, Guo Y, Lu LF, Gondek D, Wang Y, Fava RA, et al. VISTA, a novel mouse Ig superfamily ligand that negatively regulates T cell responses. *The Journal of experimental medicine.* 2011;208(3):577-92.
21. Kocoglu M, and Badros A. The Role of Immunotherapy in Multiple Myeloma. *Pharmaceuticals (Basel).* 2016;9(1).
22. Jing W, Gershan JA, Weber J, Tlomak D, McOlash L, Sabatos-Peyton C, and Johnson BD. Combined immune checkpoint protein blockade and low dose whole body irradiation as immunotherapy for myeloma. *J Immunother Cancer.* 2015;3(1):2.
23. Hallett WH, Jing W, Drobyski WR, and Johnson BD. Immunosuppressive effects of multiple myeloma are overcome by PD-L1 blockade. *Biol Blood Marrow Transplant.* 2011;17(8):1133-45.
24. Benson DM, Jr., Bakan CE, Mishra A, Hofmeister CC, Efebera Y, Becknell B, Baiocchi RA, Zhang J, Yu J, Smith MK, et al. The PD-1/PD-L1 axis modulates the natural killer cell versus multiple myeloma effect: a therapeutic target for CT-011, a novel monoclonal anti-PD-1 antibody. *Blood.* 2010;116(13):2286-94.
25. Tamura H, Ishibashi M, Yamashita T, Tanosaki S, Okuyama N, Kondo A, Hyodo H, Shinya E, Takahashi H, Dong H, et al. Marrow stromal cells induce B7-H1 expression on myeloma cells, generating aggressive characteristics in multiple myeloma. *Leukemia.* 2013;27(2):464-72.
26. Lesokhin AM, Ansell SM, Armand P, Scott EC, Halwani A, Gutierrez M, Millenson MM, Cohen AD, Schuster SJ, Lebovic D, et al. Nivolumab in Patients With Relapsed or Refractory Hematologic Malignancy: Preliminary Results of a Phase Ib Study. *J Clin Oncol.* 2016;34(23):2698-704.
27. Sonneveld P, Schmidt-Wolf IG, van der Holt B, El Jarari L, Bertsch U, Salwender H, Zweegman S, Vellenga E, Broyl A, Blau IW, et al. Bortezomib induction and maintenance treatment in patients with newly diagnosed multiple myeloma: results of the randomized phase III HOVON-65/ GMMG-HD4 trial. *J Clin Oncol.* 2012;30(24):2946-55.
28. Hulin C, Belch A, Shustik C, Petrucci MT, Duhrsen U, Lu J, Song K, Rodon P, Pegourie B, Garderet L, et al. Updated Outcomes and Impact of Age With Lenalidomide and Low-Dose Dexamethasone or Melphalan, Prednisone, and Thalidomide in the Randomized, Phase III FIRST Trial. *J Clin Oncol.* 2016.
29. Lokhorst HM, Plesner T, Laubach JP, Nahi H, Gimsing P, Hansson M, Minnema MC, Lassen U, Krejcik J, Palumbo A, et al. Targeting CD38 with Daratumumab Monotherapy in Multiple Myeloma. *N Engl J Med.* 2015;373(13):1207-19.
30. Child JA, Morgan GJ, Davies FE, Owen RG, Bell SE, Hawkins K, Brown J, Drayson MT, and Selby PJ. High-Dose Chemotherapy with Hematopoietic Stem-Cell Rescue for Multiple Myeloma. *N Engl J Med.* 2003;348(19):1875-83.
31. Seckinger A, Delgado JA, Moser S, Moreno L, Neuber B, Grab A, Lipp S, Merino J, Prosper F, Emde M, et al. Target Expression, Generation, Preclinical Activity, and Pharmacokinetics of the BCMA-T Cell Bispecific Antibody EM801 for Multiple Myeloma Treatment. *Cancer cell.* 2017;31(3):396-410.
32. Greipp PR, Miguel JS, Durie BGM, Crowley JJ, Barlogie B, Bladé J, Boccadoro M, Child JA, Avet-Loiseau H, Harousseau J-L, et al. International staging system for multiple myeloma. *J Clin Oncol.* 2005;23(15):3412-20.
33. Durie BG. Staging and kinetics of multiple myeloma. *Semin Oncol.* 1986;13(3):300-9.
34. Blade J, Samson D, Reece D, Apperley J, Bjorkstrand B, Gahrton G, Gertz M, Giralt S, Jagannath S, and Vesole D. Criteria for evaluating disease response and progression in patients with multiple myeloma treated by high-dose therapy and haemopoietic stem cell transplantation. Myeloma Subcommittee of the EBMT. European Group for Blood and Marrow Transplant. *Br J Haematol.* 1998;102(5):1115-23.
35. Seckinger A, Delgado JA, Moser S, Moreno L, Neuber B, Grab A, Lipp S, Merino J, Prosper F, Emde M, et al. Target Expression, Generation, Preclinical Activity, and Pharmacokinetics of the BCMA-T Cell Bispecific Antibody EM801 for Multiple Myeloma Treatment. *Cancer Cell.* 2017;31(3):396-410.
36. Hose D, Moreaux J, Meissner T, Seckinger A, Goldschmidt H, Benner A, Mahtouk K, Hillengass J, Rème T, Vos JD, et al. Induction of angiogenesis by normal and malignant plasma cells. *Blood.* 2009;114(1):128-43.
37. Moreaux J, Cremer FW, Reme T, Raab M, Mahtouk K, Kaukel P, Pantesco V, Vos JD, Jourdan E, Jauch A, et al. The level of TACI gene expression in myeloma cells is associated with a signature of microenvironment dependence versus a plasmablastic signature. *Blood.* 2005;106(3):1021-30.

38. Zhang XG, Gaillard JP, Robillard N, Lu ZY, Gu ZJ, Jourdan M, Boiron JM, Bataille R, and Klein B. Reproducible obtaining of human myeloma cell lines as a model for tumor stem cell study in human multiple myeloma. *Blood.* 1994;83(12):3654-63.
39. Corre J, Mahtouk K, Attal M, Gadelorge M, Huynh A, Fleury-Cappellesso S, Danho C, Laharrague P, Klein B, Rème T, et al. Bone marrow mesenchymal stem cells are abnormal in multiple myeloma. *Leukemia.* 2007;21(5):1079-88.
40. Fuhler GM, Baanstra M, Chesik D, Somasundaram R, Seckinger A, Hose D, Peppelenbosch MP, and Bos NA. Bone marrow stromal cell interaction reduces syndecan-1 expression and induces kinomic changes in myeloma cells. *Exp Cell Res.* 2010;316(11):1816-28.
41. Griewank KG, Yu X, Khalili J, Sozen MM, Stempke-Hale K, Bernatchez C, Wardell S, Bastian BC, and Woodman SE. Genetic and molecular characterization of uveal melanoma cell lines. *Pigment cell & melanoma research.* 2012;25(2):182-7.
42. Dudley ME, Wunderlich JR, Shelton TE, Even J, and Rosenberg SA. Generation of tumor-infiltrating lymphocyte cultures for use in adoptive transfer therapy for melanoma patients. *Journal of Immunotherapy.* 2003;26(4):332-42.
43. Jin J, Sabatino M, Somerville R, Wilson JR, Dudley ME, Stroncek DF, and Rosenberg SA. Simplified method of the growth of human tumor infiltrating lymphocytes in gas-permeable flasks to numbers needed for patient treatment. *J Immunother.* 2012;35(3):283-92.
44. Forget MA, Malu S, Liu H, Toth C, Maiti S, Kale C, Haymaker C, Bernatchez C, Huls H, Wang E, et al. Activation and propagation of tumor-infiltrating lymphocytes on clinical-grade designer artificial antigen-presenting cells for adoptive immunotherapy of melanoma. *Journal of immunotherapy.* 2014;37(9):448-60.
45. Hose D, Reme T, Hielscher T, Moreaux J, Meissner T, Seckinger A, Benner A, Shaughnessy JD, Barlogie B, Zhou Y, et al. Proliferation is a central independent prognostic factor and target for personalized and risk adapted treatment in multiple myeloma. *Haematologica.* 2011;96(87-95.
46. Seckinger A, Meißner T, Moreaux J, Depeweg D, Hillengass J, Hose K, Reme T, Rosen-Wolff A, Jauch A, Schnettler R, et al. Clinical and prognostic role of annexin A2 in multiple myeloma. *Blood.* 2012;120(5):1087-94.
47. Wan YW, Allen GI, and Liu Z. TCGA2STAT: simple TCGA data access for integrated statistical analysis in R. *Bioinformatics.* 2016;32(6):952-4.
48. Gilbert DF, Erdmann G, Zhang X, Fritzsche A, Demir K, Jaedicke A, Muehlenberg K, Wanker EE, and Boutros M. A novel multiplex cell viability assay for high-throughput RNAi screening. *PLoS One.* 2011;6(12):e28338.
49. Khandelwal N, Breinig M, Speck T, Michels T, Kreutzer C, Sorrentino A, Sharma AK, Umansky L, Conrad H, Poschke I, et al. A high-throughput RNAi screen for detection of immune-checkpoint molecules that mediate tumor resistance to cytotoxic T lymphocytes. *EMBO Mol Med.* 2015;7(4):450-63.
50. Boutros M, Bras LP, and Huber W. Analysis of cell-based RNAi screens. *Genome Biol.* 2006;7(7):R66.
51. Zhang C, Xin H, Zhang W, Yazaki PJ, Zhang Z, Le K, Li W, Lee H, Kwak L, Forman S, et al. CD5 Binds to Interleukin-6 and Induces a Feed-Forward Loop with the Transcription Factor STAT3 in B Cells to Promote Cancer. *Immunity.* 2016;44(4):913-23.
52. Tiedemann RE, Zhu YX, Schmidt J, Yin H, Shi CX, Que Q, Basu G, Azorsa D, Perkins LM, Braggio E, et al. Kinome-wide RNAi studies in human multiple myeloma identify vulnerable kinase targets, including a lymphoid-restricted kinase, GRK6. *Blood.* 2010;115(8):1594-604.
53. Ye DZ, and Field J. PAK signaling in cancer. *Cell Logist.* 2012;2(2):105-16.
54. Chen L, and Flies DB. Molecular mechanisms of T cell co-stimulation and co-inhibition. *Nat Rev Immunol.* 2013;13(4):227-42.
55. Algazi AP, Tsai KK, Shoushtari AN, Munhoz RR, Eroglu Z, Piulats JM, Ott PA, Johnson DB, Hwang J, Daud AI, et al. Clinical outcomes in metastatic uveal melanoma treated with PD-1 and PD-L1 antibodies. *Cancer.* 2016;122(21):3344-53.
56. Doo DW, Norian LA, and Arend RC. Checkpoint inhibitors in ovarian cancer: A review of preclinical data. *Gynecologic oncology reports.* 2019;29(48-54.
57. Raufi AG, and Klempner SJ. Immunotherapy for advanced gastric and esophageal cancer: preclinical rationale and ongoing clinical investigations. *Journal of gastrointestinal oncology.* 2015;6(5):561-9.
58. Green DR, and Ferguson TA. The role of Fas ligand in immune privilege. *Nat Rev Mol Cell Biol.* 2001;2(12):917-24.

59. Wozniak AL, Wang X, Stieren ES, Scarbrough SG, Elferink CJ, and Boehning D. Requirement of biphasic calcium release from the endoplasmic reticulum for Fas-mediated apoptosis. *J Cell Biol.* 2006;175(5):709-14.
60. Sakagami H, Kamata A, Nishimura H, Kasahara J, Owada Y, Takeuchi Y, Watanabe M, Fukunaga K, and Kondo H. Prominent expression and activity-dependent nuclear translocation of Ca2+/calmodulin-dependent protein kinase Idelta in hippocampal neurons. *Eur J Neurosci.* 2005;22(11):2697-707.
61. Swulius MT, and Waxham MN. Ca(2+)/calmodulin-dependent protein kinases. *Cell Mol Life Sci.* 2008;65(17):2637-57.
62. McIlwain DR, Berger T, and Mak TW. Caspase functions in cell death and disease. *Cold Spring Harb Perspect Biol.* 2013;5(4):a008656.
63. Parrish AB, Freel CD, and Kornbluth S. Cellular mechanisms controlling caspase activation and function. *Cold Spring Harb Perspect Biol.* 2013;5(6).
64. Alvarado-Kristensson M, Melander F, Leandersson K, Ronnstrand L, Wernstedt C, and Andersson T. p38-MAPK signals survival by phosphorylation of caspase-8 and caspase-3 in human neutrophils. *J Exp Med.* 2004;199(4):449-58.
65. Suzuki A, Kusakai G, Kishimoto A, Shimojo Y, Miyamoto S, Ogura T, Ochiai A, and Esumi H. Regulation of caspase-6 and FLIP by the AMPK family member ARK5. *Oncogene.* 2004;23(42):7067-75.
66. Alvarado-Kristensson M, and Andersson T. Protein phosphatase 2A regulates apoptosis in neutrophils by dephosphorylating both p38 MAPK and its substrate caspase 3. *J Biol Chem.* 2005;280(7):6238-44.
67. Brahmer JR, Tykodi SS, Chow LQ, Hwu WJ, Topalian SL, Hwu P, Drake CG, Camacho LH, Kauh J, Odunsi K, et al. Safety and activity of anti-PD-L1 antibody in patients with advanced cancer. *N Engl J Med.* 2012;366(26):2455-65.
68. Royal RE, Levy C, Turner K, Mathur A, Hughes M, Kammula US, Sherry RM, Topalian SL, Yang JC, Lowy I, et al. Phase 2 trial of single agent Ipilimumab (anti-CTLA-4) for locally advanced or metastatic pancreatic adenocarcinoma. *Journal of immunotherapy.* 2010;33(8):828-33.
69. Bergamaschi A, Kim YH, Kwei KA, La Choi Y, Bocanegra M, Langerod A, Han W, Noh DY, Huntsman DG, Jeffrey SS, et al. CAMK1D amplification implicated in epithelial-mesenchymal transition in basal-like breast cancer. *Mol Oncol.* 2008;2(4):327-39.
70. Pitti RM, Marsters SA, Lawrence DA, Roy M, Kischkel FC, Dowd P, Huang A, Donahue CJ, Sherwood SW, Baldwin DT, et al. Genomic amplification of a decoy receptor for Fas ligand in lung and colon cancer. *Nature.* 1998;396(6712):699-703.
71. Ashkenazi A. Targeting the extrinsic apoptosis pathway in cancer. *Cytokine Growth Factor Rev.* 2008;19(3-4):325-31.
72. Kischkel FC, Hellbardt S, Behrmann I, Germer M, Pawlita M, Krammer PH, and Peter ME. Cytotoxicity-dependent APO-1 (Fas/CD95)-associated proteins form a death-inducing signaling complex (DISC) with the receptor. *EMBO J.* 1995;14(22):5579-88.
73. Mellier G, Huang S, Shenoy K, and Pervaiz S. TRAILing death in cancer. *Mol Aspects Med.* 2010;31(1):93-112.
74. Lavrik I, Krueger A, Schmitz I, Baumann S, Weyd H, Krammer PH, and Kirchhoff S. The active caspase-8 heterotetramer is formed at the CD95 DISC. *Cell Death Differ.* 2003;10(1):144-5.
75. Nicholson DW, Ali A, Thornberry NA, Vaillancourt JP, Ding CK, Gallant M, Gareau Y, Griffin PR, Labelle M, Lazebnik YA, et al. Identification and inhibition of the ICE/CED-3 protease necessary for mammalian apoptosis. *Nature.* 1995;376(6535):37-43.
76. Powley IR, Hughes MA, Cain K, and MacFarlane M. Caspase-8 tyrosine-380 phosphorylation inhibits CD95 DISC function by preventing procaspase-8 maturation and cycling within the complex. *Oncogene.* 2016;35(43):5629-40.
77. Danial NN, and Korsmeyer SJ. Cell death: critical control points. *Cell.* 2004;116(2):205-19.
78. Li X, Wen W, Liu K, Zhu F, Malakhova M, Peng C, Li T, Kim HG, Ma W, Cho YY, et al. Phosphorylation of caspase-7 by p21-activated protein kinase (PAK) 2 inhibits chemotherapeutic drug-induced apoptosis of breast cancer cell lines. *J Biol Chem.* 2011;286(25):22291-9.
79. Bellucci R, Nguyen HN, Martin A, Heinrichs S, Schinzel AC, Hahn WC, and Ritz J. Tyrosine kinase pathways modulate tumor susceptibility to natural killer cells. *J Clin Invest.* 2012;122(7):2369-83.
80. Dunn GP, Sheehan KC, Old LJ, and Schreiber RD. IFN unresponsiveness in LNCaP cells due to the lack of JAK1 gene expression. *Cancer Res.* 2005;65(8):3447-53.

81. Parampalli Yajnanarayana S, Stubig T, Cornez I, Alchalby H, Schonberg K, Rudolph J, Triviai I, Wolschke C, Heine A, Brossart P, et al. JAK1/2 inhibition impairs T cell function in vitro and in patients with myeloproliferative neoplasms. *Br J Haematol.* 2015;169(6):824-33.
82. Schonberg K, Rudolph J, Vonnahme M, Parampalli Yajnanarayana S, Cornez I, Hejazi M, Manser AR, Uhrberg M, Verbeek W, Koschmieder S, et al. JAK Inhibition Impairs NK Cell Function in Myeloproliferative Neoplasms. *Cancer Res.* 2015;75(11):2187-99.

Figure Legends

Figure 1. Assessment of immune-checkpoint controls for the HTP-screen. (A) Representative FACS data of at least three independent experiments. Left: Expression of HLA-A2, PD-L1, CCR9 and GFP on KMM-1 cells. Right: PD-1 expression on $CD4^+$ and $CD8^+$ MILs. Isotypes are shown in dark grey. **(B)** IFN-γ-ELISA. MILs and Survivin TC clones were used as negative controls. Anti-CD3/anti-CD28-stimulated T cells were used as positive controls. **(C and E)** Luciferase-based killing assay of siRNA-transfected KMM-1 cells upon MILs co-culture. Statistical significance was calculated compared to scr1. **(D)** qPCR analysis: Knockdown efficiency of CCR9 and PD-L1 in KMM-1 cells. **(B, C, D, E)** Graphs show mean +/- SEM of at least two independent experiments. P-values were calculated using unpaired two-tailed student´s t-test. * $p < 0.05$, ** $p < 0.01$, *** $p < 0.001$, **** $p< 0.0001$

Figure 2. Performance of the HTP screen. (A) Dot plots showing technical replicates plotted against each other of normalized and scored RLUs of KMM-1 cells transfected with control siRNAs. Luciferase-independent (left) and luciferase-based (right) screening assay performed on KMM-1 -wt and -luc cells respectively. Blue dots: cytotoxicity setting. Red dots: viability setting. Pearson correlation (r^2) between the two replicate values was calculated for each setting. **(B)** Quadrant plot showing z-scores of gene knockdown KMM-1-luc cells after co-culture with MILs (cytotoxicity z-score) or culture medium (viability z-score). **(C)** Gene ranking diagram showing differential score between cytotoxicity and viability z-scores using local regression (LOESS) rank. The upper panel classifies the potential negative immune modulators with a high loess score. **(D, E)** Luciferase-based secondary screening. Knockdown tumor cells were co-cultured with (D) MILs or (E) supernatant of anti-CD3/anti-CD28 activated MILs. RLUs were normalized to Mock control. Log2 scale of cytotoxicity/viability ratio is depicted. Experiments were performed in duplicates. Mean is shown.

Figure 3. Validation of siCAMK1D effect. (A) KMM-1-luc cells were transfected using single (s1, s2, s3) or pooled siRNAs targeting CAMK1D. Scr and siCCR9 siRNAs were used as negative and positive controls respectively. Tumor cell lysis was measured using the luciferase-based cytotoxicity assay. Values were normalized to scr in each setting. **(B, C)** KMM-1 cells were transfected with the specified siRNAs sequences and 48h later (B) mRNA expression was determined by qPCR and (C) protein expression was measured via western blot. The Sodium-Potassium ATPase was used as housekeeping gene. **(D)** Live cell-imaging analysis. siRNA transfected tumor cells were co-cultured with MILs. YOYO-1 dye was added as an indicator of apoptosis (green color). The graph shows the green object counted (GCO). The experiment is representative of three independent experiments. Right: Representative pictures of scr and siCAMK1D transfected KMM-1 cells stained with YOYO-1 and co-cultured with MILs. **(E)** Luciferase-based killing assay for detection of T cell-mediated cytotoxicity in the presence of the indicated concentrations of anti-MHC-I antibody (red line) and IgG2a isotype as positive control (black line). Anti-MHC-I antibody was added to KMM-1 cells in the absence of T cells as negative control (grey line). **(F)** KMM-1-luc were pulsed with 0,005µg/ml of flu peptide 1h before flu TC co-culture or medium control. Tumor lysis was measured by luciferase assay. **(G)** End-point PCR analysis of CAMK1D expression in U266 cells. KMM-1 cells were used as positive control. **(H)**

qPCR analysis of CAMK1D knockdown efficiency in KMM-1 and U266 cells. **(I)** Live cell-imaging analysis. Scr and siCAMK1D transfected U266 tumor cells were co-cultured with MILs. No MILs-condition served as viability control. Tumor cell death was measured by the addition of YOYO-1. Columns show the green object counted (GCO). **(J)** CAMK1D expression by gene expression profiling in human MBC, PPC, BMPC, MGUS, MM and HMCL.*; ($p < 0.05$). **; ($p < 0.01$). ***; ($p < 0.001$). **(A, B)** Graphs show mean +/- SEM. Cumulative data of at least two independent experiments. **(D)** Graph shows mean +/- SEM. P-value was calculated using paired two-tailed student´s t-test. **(E)** Representative data of at least three independent experiments. Graph shows mean +/- SD. **(F, H, I)** Representative data of at least two independent experiments. Graphs show mean +/- SEM. P-values were calculated using unpaired two-tailed student´s t-test. * $p < 0.05$, ** $p < 0.01$, *** $p < 0.001$, **** $p< 0.0001$

Figure 4. Effect of CAMK1D knockdown in different tumor entities. (A) Representative FACS analysis of Fas, DR4, DR5, TNFR1 and TNFR2 expression in KMM-1 cells. Positive tumor cells are marked in orange. Isotype is shown in grey. **(B)** Representative results of siRNA transfected KMM-1-luc cells treated with recombinant FasL, TRAIL or TNF. Luciferase activity was measured after 20h of treatment. **(C)** Representative FACS analysis of FasL, TRAIL and TNFa expression on $CD4^+$ and $CD8^+$ MILs. Isotypes are shown in grey. **(D)** Luciferase-based assay: scr or siCAMK1D transfected KMM-1 were co-cultured with MILs in the presence of FasL neutralizing (anti-FasL) antibody or isotype control. Loss of luciferase activity was measured. **(E)** FACS analysis of Fas expression (shown in orange) in U266 cells. Isotype is shown in grey. **(F)** Live cell-imaging analysis. siRNA transfected U266 cells were stained with YOYO-1 and treated with rHuFasL. The experiment is representative of three independent experiments and shows the green objects counted (GCO). **(G)** Representative FACS analysis of Fas expression in PANC-1, MCF-7, Mel270 and KMM-1 cells. Positive tumor cells are marked in orange. Isotype is shown in grey. **(H)** End-point PCR of CAMK1D in Mel270. KMM-1 cells were used as positive control. **(I)** Live cell-imaging analysis of UVM cells transfected with siCAMK1D or scr siRNAs upon exposure to rHuFasL or culture medium as performed in F. The experiment is representative of two independent experiments. Values denote mean ± SEM. **(J)** Kaplan-Meier curves displaying the correlation between CAMK1D expression and patients' survival probability in Fas high and low samples. Results were generated using TCGA clinical data. Significance was calculated using the log-rank test. **(K)** Correlation between CAMK1D and PD-L1 in UVM. **(B, D, F)** Graphs show mean +/- SD. **(B, D**) P-values were calculated using unpaired two-tailed student´s t-test. **(F, I)** P-value was calculated using paired two-tailed student´s t-test**.** * $p < 0.05$, ** $p < 0.01$, *** $p < 0.001$, **** $p< 0.0001$

Figure 5. CAMK1D regulation. (A) Caspase-3, -6 and -7 knockdown in KMM-1 cells measured via end-point PCR. **(B)** Effector caspases were knocked down alone or in combination with CAMK1D and treated with rHuFasL or culture medium. Representative result of luciferase-based read-out of three independent experiments. **(C)** Intracellular calcium response in KMM-1 cells upon (top) MILs co-culture and (bottom) rHuFasL treatment. **(D)** Representative picture of intracellular free Ca^{2+} measurement in KMM-1 scr-transfected cells before (top) and after (bottom) co-culture with MILs or treated with rHuFasL. **(E)** KMM-1 cells were treated with different concentrations of CaM inhibitor and tumor cell survival was measured by luciferase activity. **(F)** scr and siCAMK1D transfected KMM-1 cells were treated as in E together with rHuFasL. **(G)** KMM-1 (left) and Mel270 (right) cells were treated with the indicated concentration of QPP-A and exposed to rHuFasL or medium. Tumor cell survival was measured by luciferase activity. **(H)** MC38-Camk1d KO and -NTS cells were each injected in C57BL6 and NSG mice. Graphs show mean ± SEM and statistical significance was calculated using two-way ANOVA Bonferroni post-hoc test. **(B)** Graphs show mean ± SD. Statistical significance was calculated using unpaired, two-tailed Student's t-test. **(E, F, G)** Experiments were performed in triplicates and representative results of three independent experiments are shown. Graphs show mean ± SEM and statistical significance was calculated using unpaired, two-tailed Student's t-test. * $p \leq 0.05$; ** $p \leq 0.01$; *** $p \leq 0.001$; **** $p \leq 0.0001$.

Figure 6. Pathways regulated by CAMK1D. (A-C) Luminex assays measuring apoptosis proteins. CAMK1D-proficient and -deficient cells were stimulated with rHuFasL for the indicated time frames. Protein expression was normalized to GAPDH and compared to scr-unstimulated cells. The amount of **(A)** cleaved caspase-8 **(B)** cleaved caspase-9 and **(C)** cleaved caspase-3 was measured. Graphs show cumulative data of at least two independent experiments. **(D)** FACS analysis of scr and siCAMK1D transfected KMM-1 cells treated for the given time frames with rHuFasL. Gate marks active caspase-3 labeled cells. **(E, F)** KMM-1 cells were treated as in (A-C) and full-length and cleaved (E) caspase-3 and (F) caspase-6 were measured via western blot. The Sodium-Potassium ATPase was used as housekeeping gene. Representative results of at least two independent experiments. **(G, H)** Representative blots showing co-immunoprecipitation of CAMK1D with **(G)** caspase-3 and **(H)** caspase-6 upon 4h rHuFasL stimulation in KMM-1 cells. Unstimulated cells were used as negative control. Unstimulated and stimulated cell lysates were used as positive control for CAMK1D detection. **(I, J)** Western blot measuring phosphorylated caspase-3 and caspase-6 upon rHuFasL stimulation. **(K, L)** Quantification of (K) phosphorylated caspase-3 and (L) phosphorylated caspase-6 upon rHuFasL stimulation for the indicated time frames. Graphs show cumulative data of four independent experiments. **(A, B, K, L)** Graphs show mean ± SEM **(C)** Graph shows mean ± SD. **(A, B, C, K, L)** Statistical significance was calculated using unpaired, two-tailed Student's t-test. * $p \leq 0.05$; ** $p \leq 0.01$; *** $p \leq 0.001$; **** $p \leq 0.0001$.

Figure 1

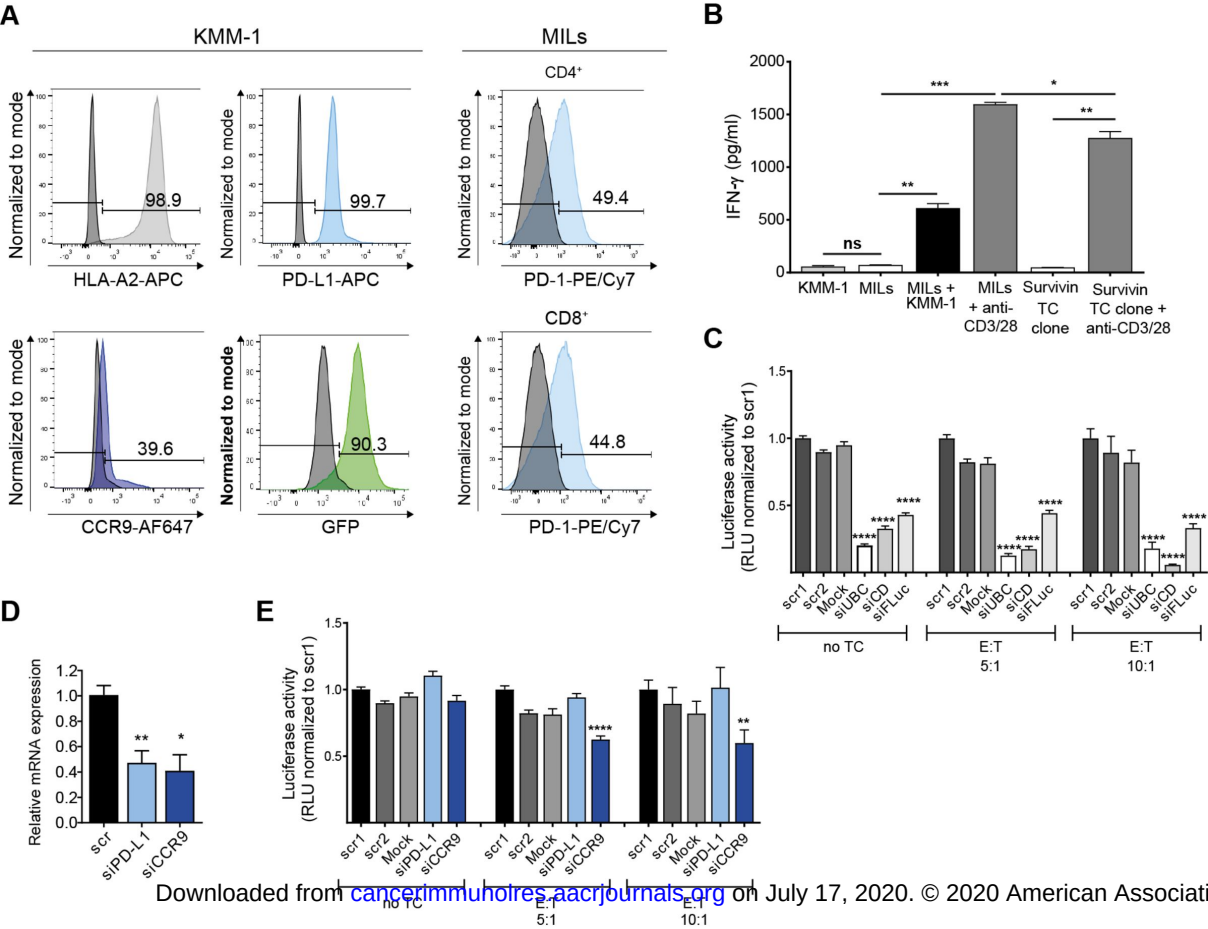

Figure 2

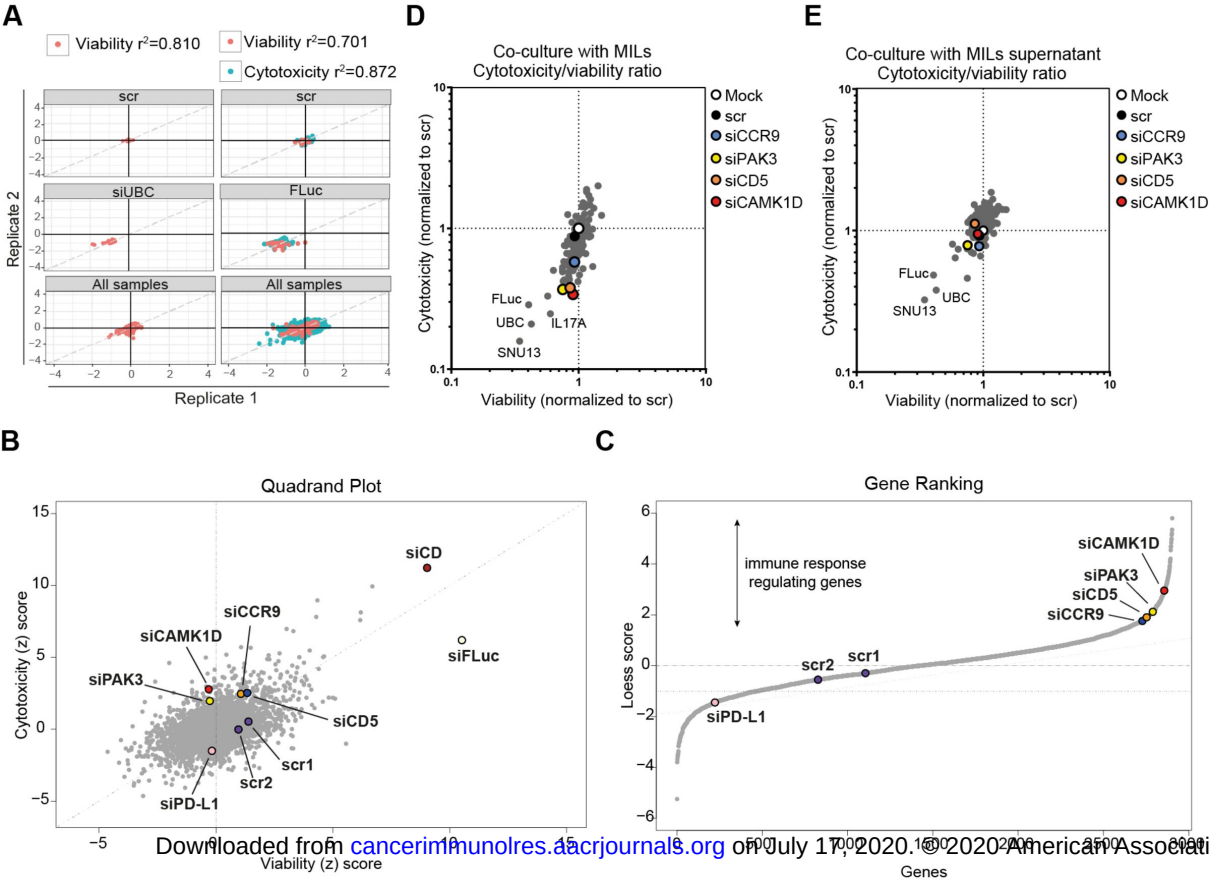

Figure 3

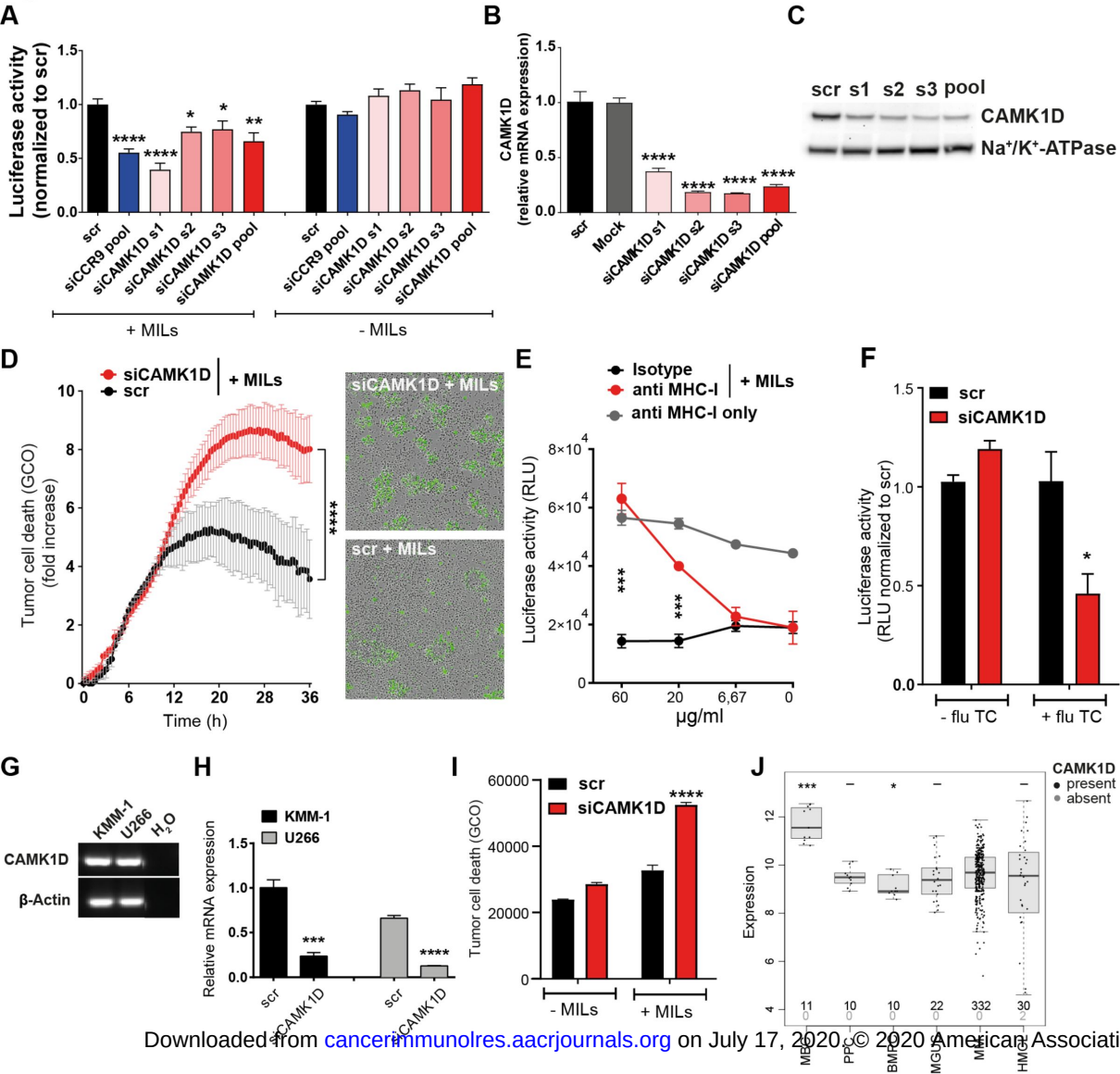

Figure 4

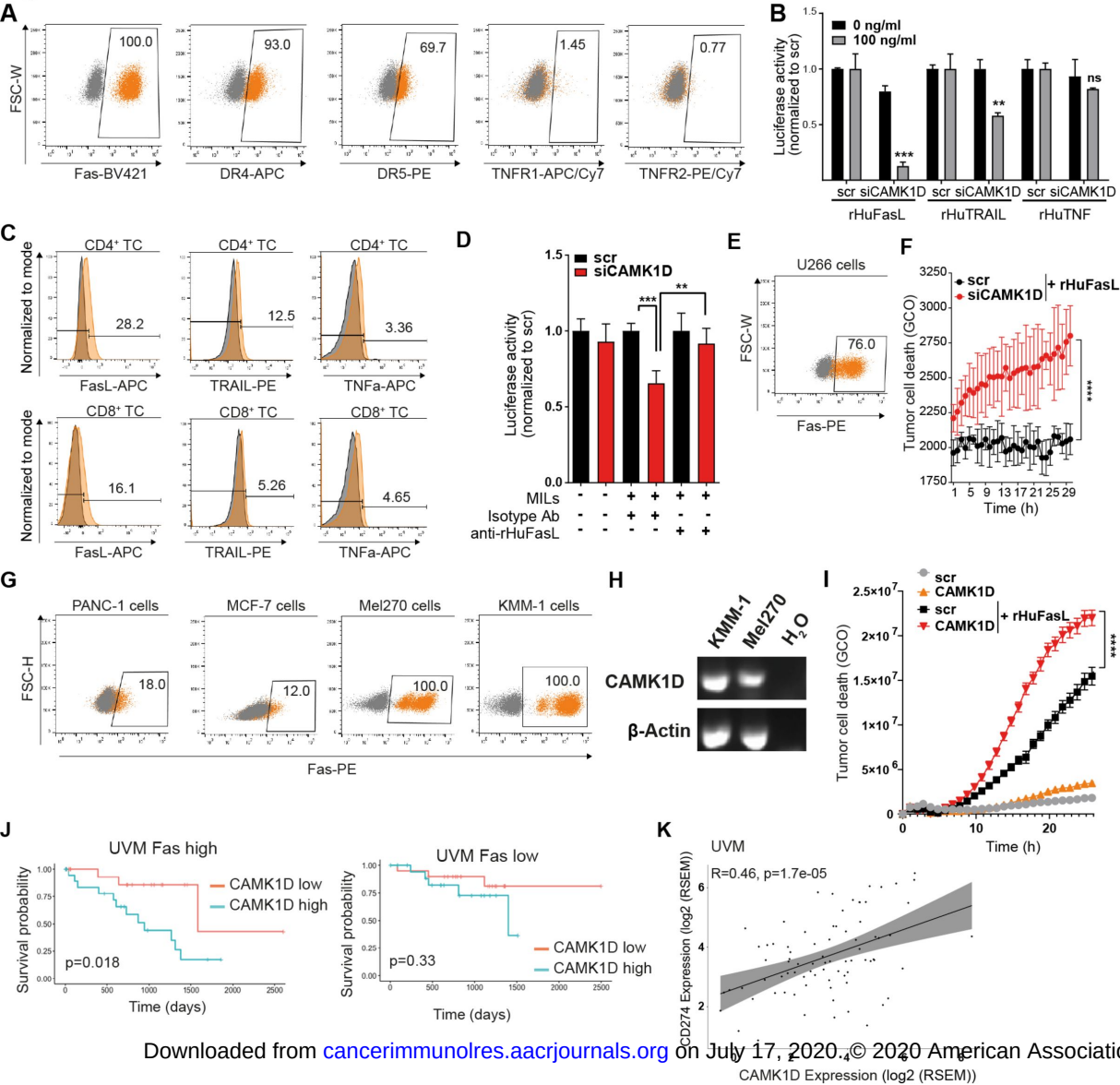

Figure 5

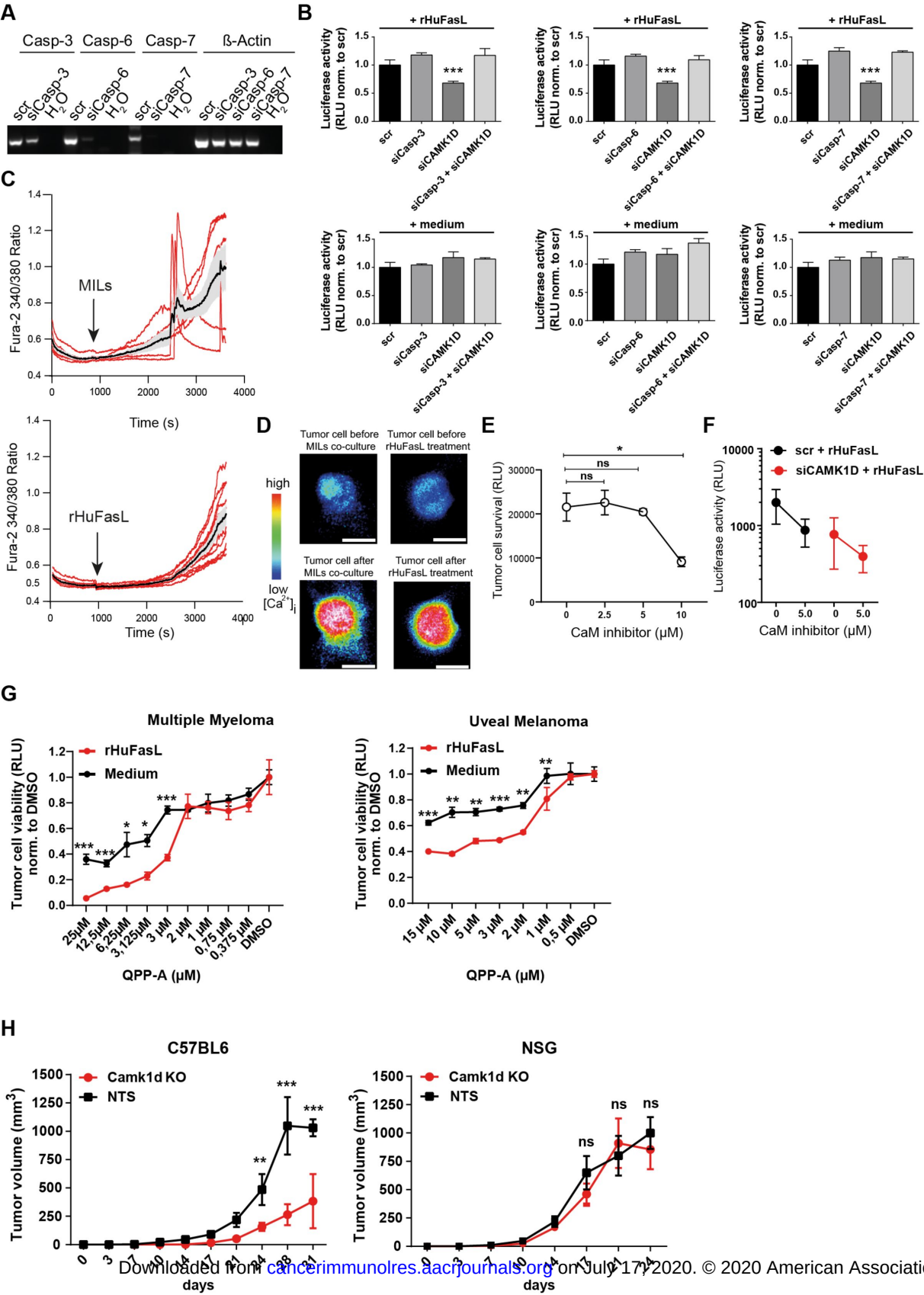

Figure 6

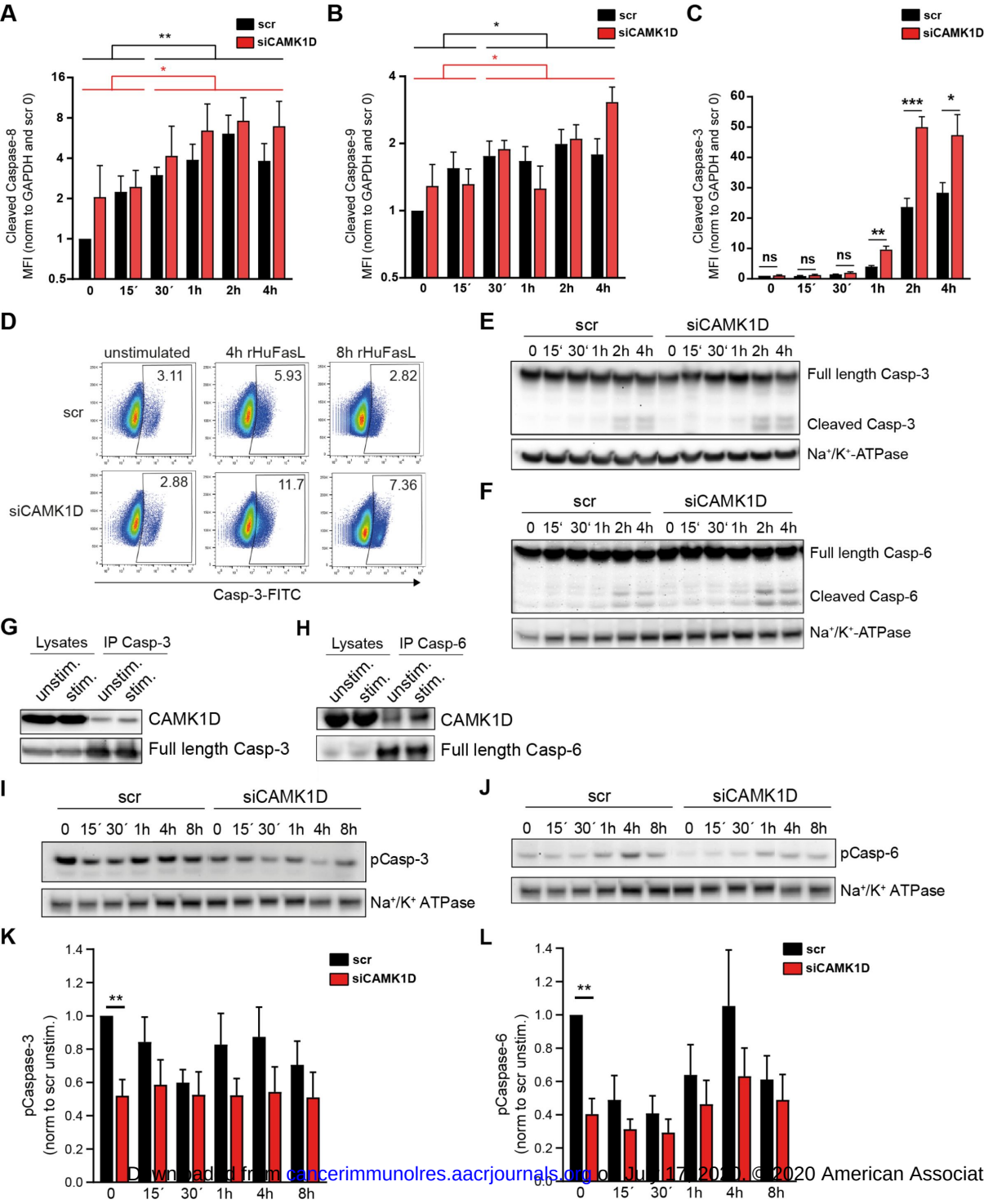

AACR American Association for Cancer Research

Cancer Immunology Research

CAMK1D triggers immune resistance of human tumor cells refractory to anti-PD-L1 treatment

Valentina Volpin, Tillmann Michels, Antonio Sorrentino, et al.

Cancer Immunol Res Published OnlineFirst July 14, 2020.